Materials Horizons

ROYAL SOCIETY OF CHEMISTRY

REVIEW

View Article Online
View Journal | View Issue

Cite this: *Mater. Horiz.*, 2023, **10**, 722

Preparation, properties and applications of two-dimensional superlattices

Fei Xing,†[a] Guangmin Ji,†[a] Zongwen Li,†[a] Weiheng Zhong,[b] Feiyue Wang,[d] Zhibo Liu,*[c] Wei Xin*[b] and Jianguo Tian[c]

Received 28th September 2022,
Accepted 6th December 2022

DOI: 10.1039/d2mh01206e

rsc.li/materials-horizons

As a combination concept of a 2D material and a superlattice, two-dimensional superlattices (2DSs) have attracted increasing attention recently. The natural advantages of 2D materials in their properties, dimension, diversity and compatibility, and their gradually improved technologies for preparation and device fabrication serve as solid foundations for the development of 2DSs. Compared with the existing 2D materials and even their heterostructures, 2DSs relate to more materials and elaborate architectures, leading to novel systems with more degrees of freedom to modulate material properties at the nanoscale. Here, three typical types of 2DSs, including the component, strain-induced and moiré superlattices, are reviewed. The preparation methods, properties and state-of-the-art applications of each type are summarized. An outlook of the challenges and future developments is also presented. We hope that this work can provide a reference for the development of 2DS-related research.

1. Introduction

The research on superlattices can be traced back to the late 1960s.[1] In order to observe the Bloch oscillation of electrons, people initially predicted and designed a novel material which was periodically arranged with two different semiconductors in a sequence.[2] The band alignments of the two require a spatial distribution usually exhibited as a multiple quantum well. The size of each composition is kept only several or tens of times larger than that of the lattice constants but shorter than the de Broglie wavelengths of electrons.[3] This makes the overlap between wave functions in adjacent wells more obvious,

[a] *School of Physics and Optoelectronic Engineering, Shandong University of Technology, Zibo, 255049, China*
[b] *Key Laboratory of UV-Emitting Materials and Technology, Ministry of Education, Northeast Normal University, Changchun, 130024, China. E-mail: xinwei@nenu.edu.cn*
[c] *Key Laboratory of Weak Light Nonlinear Photonics, Ministry of Education, Teda Applied Physics Institute and School of Physics, Nankai University, Tianjin, 300071, China. E-mail: liuzb@nankai.edu.cn*
[d] *State Key Laboratory of Optoelectronic Materials and Technologies, School of Electronics and Information Technology, Sun Yat-sen University, Guangzhou, 510275, China*
† These authors contributed equally.

Zhibo Liu

Zhi-Bo Liu is a professor at the Key Laboratory of Weak Light Nonlinear Photonics, Ministry of Education, School of Physics and Teda Institute of Applied Physics, Nankai University, China. He received his PhD degree from Nankai University, China, in 2006. His current research interests include nonlinear optics, 2D materials, and optical sensors.

Wei Xin

Wei Xin received his BS (2010) from the Changchun University of Science and Technology and PhD (2017) from Nankai University. After that, he continued his research in the State Key Laboratory of Applied Optics, Changchun Institute of Optics, Fine Mechanics and Physics, Chinese Academy of Sciences. In 2020, he joined Northeast Normal University as an associate professor in the Key Laboratory of UV-Emitting Materials and Technology, Ministry of Education. His research focuses on 2D material-based micro/nanodevices and laser processing.

resulting in the unique properties of carriers different from those in traditional bulk materials and presenting broad application prospects.[4,5] This class of materials are called superlattices, and they've been getting a lot of attention since they were proposed. New elements are constantly added to push the field forward especially after the appearance of two-dimensional (2D) materials.[6,7] The concept of integrating them into a new 2D superlattice (2DS) has given another impetus to their development.[8–11]

In a broader sense, a 2D material refers to a film with atomic thickness in the out-of-plane direction. More than thousand kinds have been predicted so far.[12,13] From the perspective of element types forming the layer, 2D materials have been divided into mono- (such as graphene, black phosphorus (BP) *etc.*) or multiple-element (hexagonal boron nitride (h-BN), transition metal dichalcogenide (TMD) *etc.*) ones. Regardless of the material, the intralayer atoms are always held together by chemical bonds, and the neighbor layers are bonded to each other by the relatively weak van der Waals (vdW) forces.[13–15] This dangling-bond-free lattice makes it technically easy to stack multiple 2D materials arbitrarily, so the forms of 2D "component superlattices" (CSs) are initially designed just in imitation of the traditional layer-by-layer structures.[16–19] However, natural advantages of 2D materials in their properties, dimension, diversity and compatibility present more possibilities for their further performance breakthrough. With in-depth research, other types such as the in-plane CS, "strain-induced superlattice" (SS) and "moiré superlattices" (MS) appear one after another.[20–23] The performances of carriers in these types are compressed from three to two dimensions. This conceptional expansion is not mechanical duplication but makes use of both the material's properties and structural characteristics at a micro/nano scale. 2DSs contribute to further expanding the performance of electronic components and downscaling the size of related devices, so as to expand Moore's law to the field of optoelectronics.

Fig. 1 gives a brief introduction of the above three typical 2DSs which covers most of the existing structural systems. Their main characteristics can be summarized as follows:

(1) CS: similar to the structure of traditional superlattice materials, CS is usually arranged by different kinds of 2D materials periodically in the out-of-plane or in-plane directions.[19,20] The atomic monoelemental crystals or even their composite films with thicker thicknesses are selected as building blocks depending on the field of applications. This structure is currently the dominant configuration of 2DSs. The interfacial effect and energy band alignment of each element are generally the decisive factors affecting the performance of related devices.

(2) SS: the SS can be considered as an evolution from the basic structure of the CS. When people studied the traditional GaAs/GaAsP superlattice in as early as the 1980s, they found that strain/stress is common and non-negligible, affecting the properties of materials once the lattice mismatch was greater than ~0.1%.[24] With the study of 2D materials being continued recently, it is found that it is impossible to avoid the periodic interfacial buckling especially when the strain in the materials exceeds a critical value (~2–3%).[25,26] In this case, the strain is more important and can induce more novel phenomena. These morphological changes are also accompanied by the introduction of localized fields, which can further modulate the band structures of materials in the in-plane direction.[27,28] At present, there are still few reports on SSs and there is no unified standard to define the structures. Whether the band structure of a material is subject to periodic modulation caused by external substances is the main issue here. We collectively refer to the 2DSs with the above characteristics as SSs.

(3) MS: the MS can be considered as a further extension of SS, and recently it has been extensively studied as a

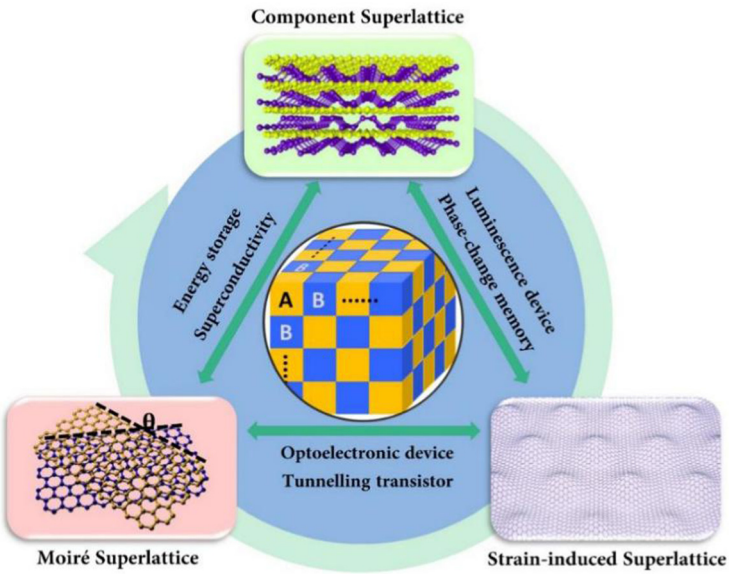

Fig. 1 Schematic diagram of 2DSs, including their formations and potential applications.

separate system.[29–32] The MS is usually made by stacking two or more layers of the same or different kinds of 2D materials together with a relative twisted angle (θ) between layers. It causes an interlayer mismatch in the lattice and a periodic angle-dependent moiré potential along with the moiré patterns in a larger area. This potential affects the energy band structure of the system as a whole, leading to the novel physical phenomena different from the traditional superlattices.

Significantly, we can find that there is no complete boundary in the morphology between the above-mentioned different 2DSs. The existence of multiple influencing factors in a certain system can even be observed. Although the final properties of a 2DS are determined synthetically, the dominant role is still relatively clear. As a typical example, when designing a light emitting diode (LED) device by using a CS system, Novoselov's group was more concerned with the influence of energy band alignment and the tunneling movement of carriers in it rather than the effects of lattice mismatch.[33] In another experiment, Mao *et al.* identified the influence of strain and ruled out the moiré potential interpretation even though the moiré patterns were clearly between the G/$NbSe_2$ interfaces.[26] Therefore, based on the main factors affecting the properties of 2DSs, we sorted out and discussed the recent work accordingly.

The research on 2DSs is an emerging field. Although there were many published reviews, most of them paid more attention to the properties and applications of a selected type. There is a lack of overview introduction about 2DSs at present. In addition, due to their similar architectures to the 2D heterostructures and metamaterials, there is usually confusion in the discussion of concept of 2DSs. Whether the de Broglie wave of carriers in a material can be effectively modulated by the periodic potential field is an important criterion for judging as a 2DS. Based on this, we summarize the recent research studies and reorganize them from the perspective of preparation, properties and applications of different 2DSs. Following that, the existing challenges and development are also discussed. We hope that this review can provide beneficial reference for the development of follow-up work.

2. Preparation strategies of 2DSs

Preparing high-quality 2DSs is critical because it is the basis for later applications. Natural vdW superlattices can be separated from minerals, but the materials got in this way are usually having single properties.[34,35] Artificial 2DSs is still the dominant objective. Inspired by preparation of 2D heterostructures, preparing 2DSs can also follow the top-down and bottom-up synthetic strategy.[10,36] The advantage of the former is that we can arrange different materials in order as desired, but it is relatively inefficient and inflexible. In contrast, the latter is simpler but the materials involved are usually limited. How to integrate the advantages in new strategies has always been the focus. Here, by summarizing the common preparation strategies for 2DSs, we briefly introduce three main methods, including the mechanical transfer, gas vapor growth and liquid-assisted engineering. These methods run through the development history of 2DSs and the preparation efficiency and qualities of 2DSs have improved greatly (Fig. 2).[37–50]

2.1 Mechanical transfer

Like playing with LEGO, 2D materials can be treated as building blocks and assembled with one-atomic-plane precision as designed.[16–18] Generally, two aspects need to be considered during mechanical transfer: high-quality exfoliation of materials and subsequent stacking (Fig. 3a).[18] The great success of exfoliating graphene in experiment by Geim *et al.* encourages people to push the method to improve day by day.[12] With continuous technical optimization recently, many techniques, including the liquid exfoliation, gold-assisted exfoliation *etc.*, have emerged one after another.[51–55] The variety of materials obtained has been enriched largely under premise of ensuring high lattice quality, and the sample size can range from microns to even centimetres. For example, under the guidance of adhesive energies to gold surface, Gao's group exfoliated more than 40 types of single-crystalline monolayer 2D materials at the same time.[54] Both high lattice quality and excellent properties were exhibited.

After obtaining the high-quality 2D materials, the next is to stack them artificially. Due to the high degree of spatial freedom, the type, sequence, position or even twisted angle between layers can be controlled well. Taking the preparation of an out-of-plane vdW heterostructure as an example, mechanical transfer generally goes through the following process:[56] first, the same type or different types of materials I and II (MI/MII) are exfoliated from its bulk to two pieces of Si/SiO_2 substrates, respectively. The MI is chosen as the bottom layer, and the MII as the upper needs to further cover a transition film composed of a water-soluble polymer and a polymethyl methacrylate (PMMA) materials. Second, the silicon slice containing MII is immersed in a bath and the PMMA with MII can be obtained from the water surface after dissolving the polymer. With the help of a microscope operation system, this film can be transferred to another slice to keep MII aligned on top of MI precisely. Finally, the I/II vdW heterostructure is successfully fabricated after dissolving the PMMA in acetone and annealing the sample at a high temperature in a protective gas environment to ensure close contact between the interfaces.

The above procedure can be regarded as the basis for preparing vdW structures. Preparing 2DSs is just an extension of it, and just certain operations need to be adjusted as designed. For example, preparing CSs requires repetition of the procedure, while MSs are concerned more about the twisted angle between the upper and lower materials. As for the SSs that need to undergo buckling transitions between 2D materials or even between materials and substrates, in the mechanical transfer process more attention should be paid to the interlayer coupling, which determines whether the subsequent samples can exhibit excellent properties. To ensure this, in a typical work reported by Andrei's group, a sandwiched graphene/nanopillar/h-BN structure was annealed overnight in an environment of high temperature and protective gas.[57] Recently, with continuous optimization, the quality and efficiency during

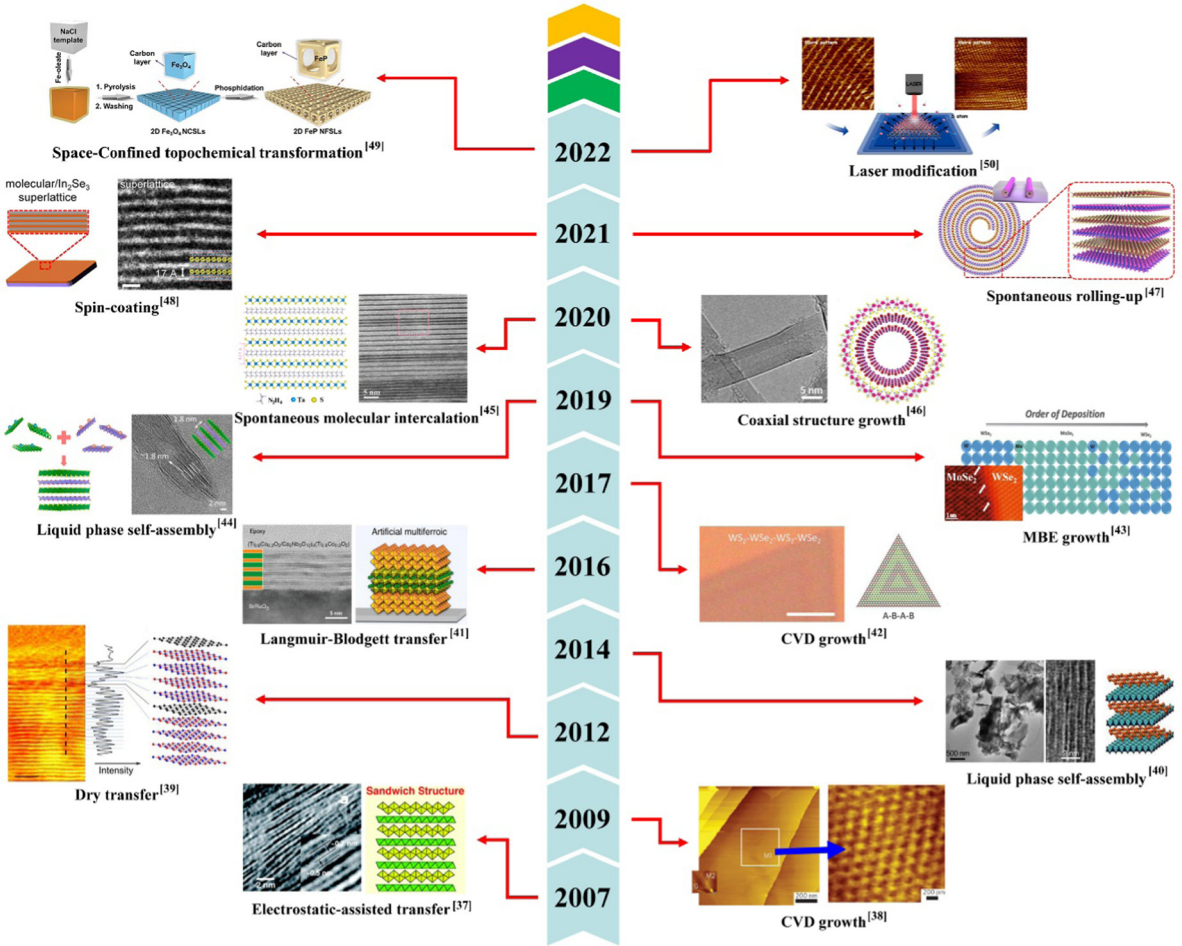

Fig. 2 Timeline showing the development of the preparation of 2DSs. Reproduced with permission.[37–50] Copyright 2008, 2012, 2013, 2014, 2015, Nature Publishing Group. Copyright 2012, 2013, American Chemical Society. Copyright 2013, 2015, 2016, Wiley-VCH. Copyright 2017, American Association for the Advancement of Science. Copyright 2021, Elsevier.

transfer are improved greatly, making the preparation of 2DSs technically easier (Fig. 3b).[58] The liquid surface pressure and surface energy are considered to facilitate large-area and high-quality transfer of materials, and the transition film has been replaced by polydimethylsiloxane (PDMS) or others for reducing residues.[59–62] The treatment of the substrate is also one of the important factors affecting the transfer. As an example, with the aid of bubbles and capillary bridges between graphene and substrate, Gao *et al.* realized the face-to-face transfer of wafer-scale graphene films successfully.[63]

Mechanical transfer is common in the preparation of vdW structures. It has obvious advantages in the architecture design and implementation in space. Due to the high quality of 2D materials obtained by exfoliation, the heterostructures or even 2DSs prepared in this way usually exhibit excellent properties. However, the complicated operation and low sample yields are the main difficulties. It is mostly confined to the laboratory and fails to integrate with the industrial techniques although the techniques have improved tremendously.[50] Combination with other methods is the inevitable trend of future development. For example, recently, Kim's group has reported a programmed crystal assembly technique which combines mechanical transfer and gas vapor growth to prepare wafer-scale 2DSs.[64]

2.2 Gas vapor growth

Gas vapor growth is one of the most developed methods to prepare large-area, high-quality 2D materials or 2DSs. It is more compatible with existing semiconductor processing techniques, endowing it with great potential for industrial applications, especially in the field of optoelectronics. Here, two important growth techniques, including chemical and physical vapor deposition (CVD, PVD) are reported. Different from the previous method of preparing 2D materials, here we mainly focus on the preparation of 2DSs.

2.2.1 Chemical vapor deposition (CVD) growth. The CVD technique tends to be specialized gradually. Its general operation procedure can be described as follows:[13,65–68] first, the gaseous or solid precursors are fed into a tube furnace. Then, by regulating the flow of gas, temperature and pressure, the precursors react chemically and nucleate at the reaction zones on a target substrate. Finally, the nucleation increases gradually to form flakes or even a film. This procedure does not appear to

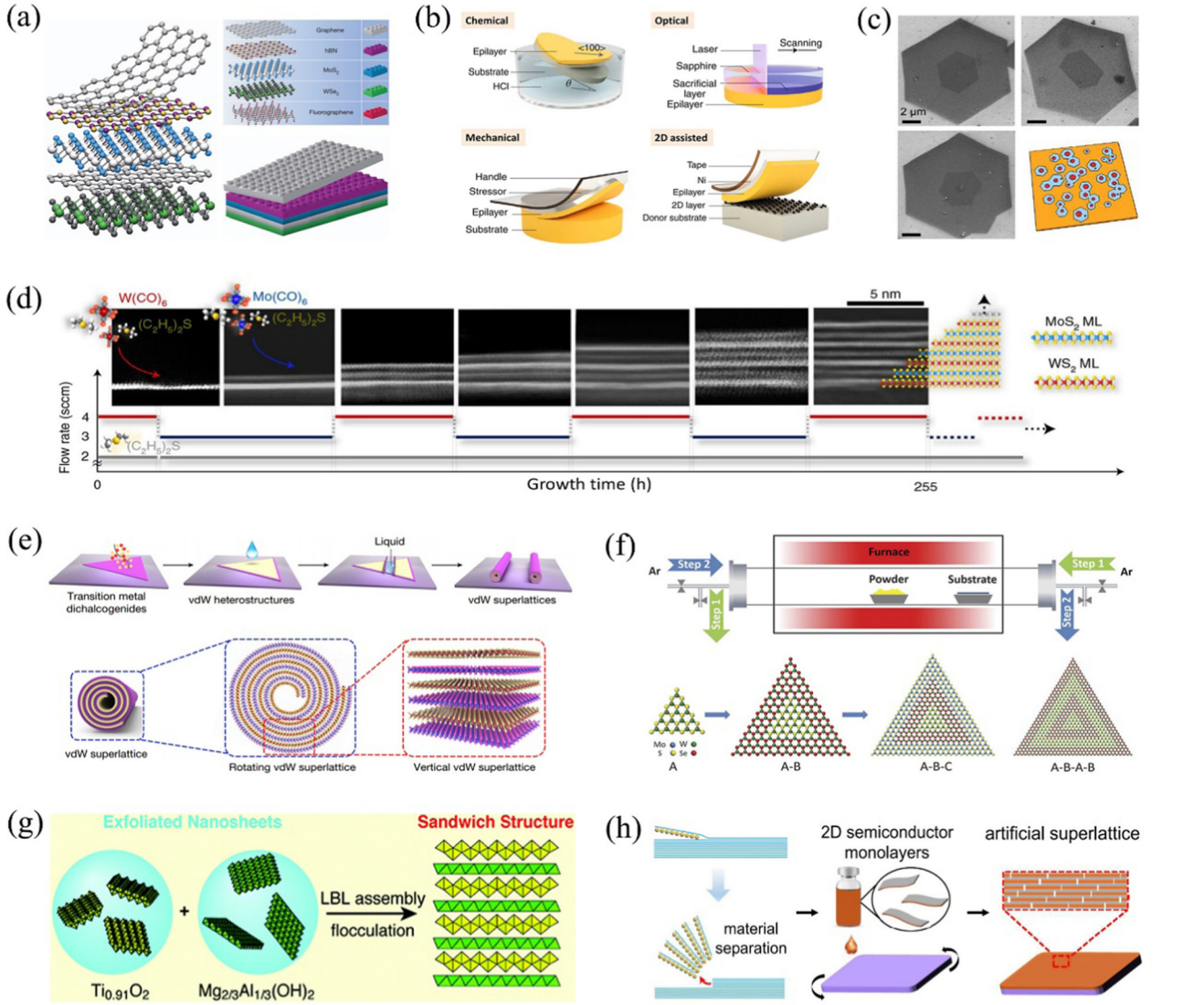

Fig. 3 (a) vdWs heterostructures and their Lego block analogies. Reproduced with permission.[18] (b) Schematic of common exfoliation-transfer techniques. This process sometimes needs to be assisted by chemical etching or laser heating operations. Reproduced with permission.[58] (c and d) Optical and scanning transmission electron microscope (STEM) images of out-of-plane vdWs heterostructure, MS and layer-by-layer CS samples prepared by CVD technique. Reproduced with permission.[70,74] (e) Fabrication schematic of the roll-up CSs. Reproduced with permission.[47] (f) Growth of in-plane CSs with a modified CVD technique. Reproduced with permission.[42] (g) Inorganic-sandwich CSs periodically deposited by layered double hydroxide and oxide nanosheets with a LBL assembly technique. Reproduced with permission.[37] (h) Schematic of the assembled tetraheptylammonium bromide-capped In_2Se_3 monolayers through complete intercalation, separation and spin-coating process. Reproduced with permission.[48] Copyright 2013, 2019, 2021, Nature Publishing Group. Copyright 2017, American Association for the Advancement of Science. Copyright 2007, 2013, American Chemical Society. Copyright 2021, Elsevier.

be complicated, but obtaining the desired fine 2DSs actually requires very demanding deposition conditions.[20,42,69] In general, the environment of the chemical reaction, including pressure, temperature, nucleation space, *etc.*, the reaction procedure, including duration, sequence, times, use of additives, *etc.*, and the quality of chemical reactants, including precursors and substrates, are all factors that need to be considered. Due to the relatively rich manipulation parameters, CVD growth has been used for preparing almost all types of 2DSs mentioned above.

For instance, in 2013, Chiu's group reported the preparation of twisted-bilayer graphene (TBG) on Cu foils by using the ambient pressure CVD (AP-CVD) technique for the first time (Fig. 3c).[70] By optimizing the environment temperature, gas pressure, and the thickness and purity of the copper foils, the TBG grains and twisted angle between layers can be regulated effectively. Similar operations were also reported by Liu's group.[71–73] By further improving the purity of the copper foil while reducing the pressure in the tube furnace, the overlapping region of TBG samples can approach 100 × 100 μm^2.[72] Besides graphene, in 2014, Liu *et al.* fabricated the twisted MoS_2 bilayers on various substrates.[69] In 2021, by precisely controlling the epitaxy kinetics process, Jo's group achieved the

layer-by-layer stacking or even arbitrary rotating of TMD materials (Fig. 3d).[74] However, decreasing the nucleation rate initially and enriching the variety of stacked materials should be highlighted during the deposition. To solve this problem, Zhao *et al.* proposed a general strategy a little earlier.[47] By dropping an ethanol–water–ammonia solution onto an vdW heterostructure, a force-driven rolling-up higher order CS was synthesized (Fig. 3e). This process is relatively feasible to operate, and extends the concept of superlattices to one dimension, offering more freedom in interlayer coupling for further applications.[47,75] In addition to the 2DSs mentioned above, CVD growth also shows good performance for preparing in-plane CSs.[20,42,65] In 2015, Li *et al.* synthesized the monolayer WSe_2–MoS_2 lateral p–n junction for the first time and observed an atomically sharp interface.[68] On this basis, by controlling the reverse flow during temperature swing between successive growth steps, Zhang *et al.* deposited two types of TMD materials alternatively (Fig. 3f).[42] In another report, Xie *et al.* also synthesized the coherent monolayer 2DSs through a modulated metal–organic CVD method.[20] The supercell presented a controllable strain distribution because of the lattice mismatch between materials. In 2020, the concept of 'in-plane CS' was further extended to perovskites. By controlling ion diffusion process, Dou's group exhibited an effective method for preparing lateral perovskite 2DS first.[76] In addition, the CVD technique also provided coping strategies for preparing SSs. In 2020, by applying the low-pressure CVD (LPCVD) method, Hudson *et al.* prepared a graphene film on a polished copper foil at 1020 °C.[77] After slowly cooling the sample to 80 K, the covered graphene was arranged in periodic ripples to form a SS under the tensile and shear stresses. During this process, the cooling speed and uniformity are important for the latter properties of the SSs.

In general, the biggest advantage of the CVD technique is that it can be used to prepare large-area, high-quality 2DSs, but in the short term, a breakthrough should be made in the synthesis of vertical CS. The improvement on controlling material types, stacking sequences and twisted angles between layers should also be noticed. In addition, as a common problem faced in the CVD technique, achieving the preparation of wafer-scale single crystal is still a focus of research.

2.2.2 Physical vapor deposition (PVD) growth. PVD and CVD growths of 2DS materials are similar in the selection of precursors or operation chambers, but PVD growth rarely involves chemical reactions. The precursors concerned are usually their bulks, and the lattice matching between 2D materials or with substrates needs to be focused upon. The atoms/molecules for deposition should be arranged regularly on a specific substrate. Guided by this, in 2004, Heer's group successfully prepared thin-layer graphene on the surface of a 6H-SiC substrate.[78] 2D heterostructures or even 2DSs were also prepared later.[79,80] In 2018, by using a typical molecular beam epitaxy (MBE) method, Xie *et al.* successfully prepared an in-plane $In_{0.6}Ga_{0.4}As/In_{0.44}Al_{0.56}As$ superlattice structure.[81] Mismatched stress/strain fields have been proven to be significant in material properties. In 2020, an epitaxial growth of graphene/h-BN MS was also achieved by Beton's group.[82] The graphene first nucleated at the edge of h-BN, forming nanoribbons of controllable width, and then grew across the entire surface. Recently, another PVD technique named laser-assisted epitaxy growth has caught much attention.[83] By using this technique, Hao's group prepared high-quality, few-layer BP films of centimetre size.[84] Despite these tremendous advances, the PVD growth is still not developed sufficiently for preparing 2DSs at present. But considering the precise control of the types and thicknesses of deposited materials, it has great development potential in the future.

2.3 Liquid-assisted engineering

With the help of liquid surface pressure, chemical intercalation agents or external applied voltage, 2D materials can be exfoliated from their bulks in a liquid. By using different deposition techniques subsequently, 2DSs can be synthesized. This process is convenient to operate, but it is always limited by the material types and it is difficult to ensure a good crystal lattice quality at the same time. As an example, here we mainly introduce two techniques: liquid-assisted layer-by-layer deposition (LLD) and solution-phase self-assembly (SSA). They are representative in liquid-assisted engineering of 2DSs.

2.3.1 Liquid-assisted layer-by-layer deposition (LLD). The LLD technique is typical for preparing 2DSs based on the charge adsorption and self-assembly of nanosheets at an air–liquid interface. The colloidal suspensions of nanosheets with opposite charges are generally used as different basic components of 2DSs, and the preparation is accomplished just by immersing a substrate into different liquids sequentially.[37,41]

For example, in 2007, Li's group fabricated a composite $Ti_{0.91}O_2$/layered double hydroxide (LDH) superlattice and a $Ca_2Nb_3O_{10}$/LDH film by alternately adsorbing the negatively charged metal oxide and the positively charged double hydroxide nanosheets (Fig. 3g).[37] The thickness of different components was controlled at 0.6 nm. In contrast, for preparing 2DSs by combining materials with the same charge, a connecting agent such as the polycation/polyanion solution were applied for help. The nanopieces ($Ti_{0.8}Co_{0.2}O_2$ and $Ti_{0.6}Fe_{0.4}O_2$) were connected as 2DSs with the help of poly diallyl dimethyl ammonium chloride.[41] The electrostatic adsorption is key but not limited, so the materials for selection are fruitful.[85,86] Another important liquid-assisted deposition is the Langmuir–Blodgett transfer technique.[87] The nanosheets for deposition are first mixed with an amphiphilic organic compound and then spread over water. The hydrophilic side of the mixture is in contact with the water surface and extends away to the air. A solid-like single-molecule layer can be formed on the liquid surface as a result. By this time, by immersing in and removing out of an appropriate substrate repetitively, 2DSs with multiple components can be obtained. For example, in 2009, Akatsuka *et al.* successfully produced a high-ordered CS film on a silicon wafer and a quartz glass substrate.[88] Li *et al.* also prepared similar samples on different substrates by using this technique.[89]

2.3.2 Solution-phase self-assembly (SSA). Besides LLD, the SSA technique is also a common liquid-assisted engineering

method for preparing 2DSs. The difference is that the SSA can spontaneously intercalate 2D materials just by mixing suspensions of nanosheets with opposite charges.[19,90] Scalable and controllable 2DSs can even be prepared conveniently by adopting modified flocculation.[91] For example, the Li^+ ions were added into a suspension with manganese dioxide nanosheets for achieving turbine laminated Li–Mo oxide films.[92] 2DSs with alternating materials were prepared just by mixing differently charged metal oxides with nanosheet suspensions of a double hydroxide.[37] In 2015, Cai *et al.* even found that the different materials with the same charge can be combined to form 2DSs.[93] By adding the polycations into the nanosheet suspension with anions, the surface charges of nanosheet were modified. The newly formed electropositive and original electronegative sheets can flocculate together spontaneously. In 2019, Xiong *et al.* assembled a MoS_2/LDH 2DS *via* SSA using negatively charged MoS_2 and positively charged LDH sheets.[44] In 2021, Duan's group reported a novel SSA technique.[48] A 2DS with alternating molecular layers and inorganic 2D monolayers was obtained by intercalating tetraalkylammonium cations in a liquid, as shown in Fig. 3h. Different from the traditional SSA technique, this method can self-refresh the surface of crystal constantly, alleviating the self-delay effect of organic ammonium intercalation peeling 2D layered crystals, and greatly ensuring the integrity of large crystal intercalation. It provides a feasible, low-cost and high-yield chemical means for the preparation of 2DSs with high quality, and adjustable structure and function.

Generally speaking, the SSA technique has progressed greatly in recent years.[83] It is simple, efficient and has great development prospects. Compared with the preparation of CS materials, this technique may encounter greater obstacles in preparing MSs and SSs because of the higher requirements for lattice quality. However, a reasonable design is believed to controllably hybridize and prepare target 2DSs with special properties and applications.

3. Properties and applications

In this part, the symbolic properties and recent applications of different types of 2DSs are mainly focused. The properties of 2DSs are jointly determined by the material components and architectures, which provides rich variability and freedom for applications of related devices. It is hard to summarize regularity for this reason, so here only some common characteristics are described.

3.1 Properties and applications of CS

3.1.1 High surface-to-volume ratio and chemical applications. High surface-to-volume ratio and fast charge transfer are the most basic requirements for materials used in chemical applications, especially in the field of energy conversion. The CSs prepared by liquid-assisted engineering can meet such requirements well. In general, such CSs are composed of alternate conductive and oxidizable nanosheets.[94] The conductive sheets (*e.g.*, graphene, MXenes, and TMDs) can realize rapid charge transfer, while the oxidizable sheets (*e.g.*, transition metal oxides (TMOs) and LDHs) can provide high-capacity energy storage and efficient catalytic reactions.[94–97] The close contact between adjacent sheets facilitates interfacial interactions, resulting in a speeding up of the conversion rate and an increase in catalytic activity. Based on this, the CSs are of great value in supercapacitors, rechargeable batteries, catalysts, and so on. For example, a CS made of alternant LDH/GO/rGO sheets was reported as a supercapacitor, and a composite periodically assembled by Co-Al/Co-Ni LDH sheets and graphene was applied as the electrode.[98–100] Compared with conventional bulk materials, superlattices generally exhibit higher capacity and faster charge/discharge rate. As reported, by synthesizing a Ni-Al-LDH/GO CS cathode, Ge *et al.* improved the capacity of alkaline hybrid supercapacitors by at least two times. 72.7% of capacity was retained even after thousands of charge/discharge cycles (Fig. 4a).[95] Similarly, the enhanced capacity performance was also observed in the Ti_3C_2/Ni-*Co*-Al LDH CSs.[101]

For lithium-ion storage applications, a CS composed of TMOs is ideal because it exhibits better performance as an electrode due to higher storage capacity. Conventional electrodes are usually made of MnO_2 nanosheets. They need to undergo a conversion reaction and are inactivated during repeated charge/discharge processes.[102] If the sheets are replaced by a graphene/MnO_2 CS, the conversion of MnO_2 is constrained and the transformants can be confined in 2D channels of graphene materials. This can effectively avoid the capacity decay, greatly improving cycling stability of metal ion storage.[103] Similarly, the graphene/MnO_2 CSs also performed well in Na-ion storage. The theoretical results showed that the diffusion energy barrier generally decreases as the interlayer distance increases, suggesting that layer-expanded layered materials have higher ion mobility and could achieve faster charge and discharge kinetics.[104] Compared with the materials with randomly stacked composites, each layer of nanosheets in the superlattice maintain a large interlayer spacing, which provides more 2D channels for the rapid diffusion of metal ions, thereby obtaining superior rate capability.

The ion diffusivity D^{GITT} can be obtained *via* the formula

$$D^{GITT} = \frac{4}{\pi\tau}\left(\frac{m_B V_M}{M_B S}\right)^2\left(\frac{\Delta E_s}{\Delta E_t}\right)^2$$

where τ, m_B, M_B, V_M and S are the constant current pulse time, mass, molar weight, molar volume, and the area of electrode–electrolyte interface, respectively. ΔE_s is the decrement between original voltage (E_0) and steady-state voltage (E_s). ΔE_τ is the total change of cell voltage excluding the IR-drop during the constant current pulse τ. Accordingly, the excellent cycling stabilities after 5000 cycles with $\sim$0.004% and 0.0078% capacity decay per cycle were respectively obtained for Li^+ and Na^+ storage in experiments.[105] In contrast, anodes composed of other TMO/TMD-graphene CSs also show potential in energy storage.[106,107] The N-doped graphene/$Ti_{0.87}O_2$ was prepared as

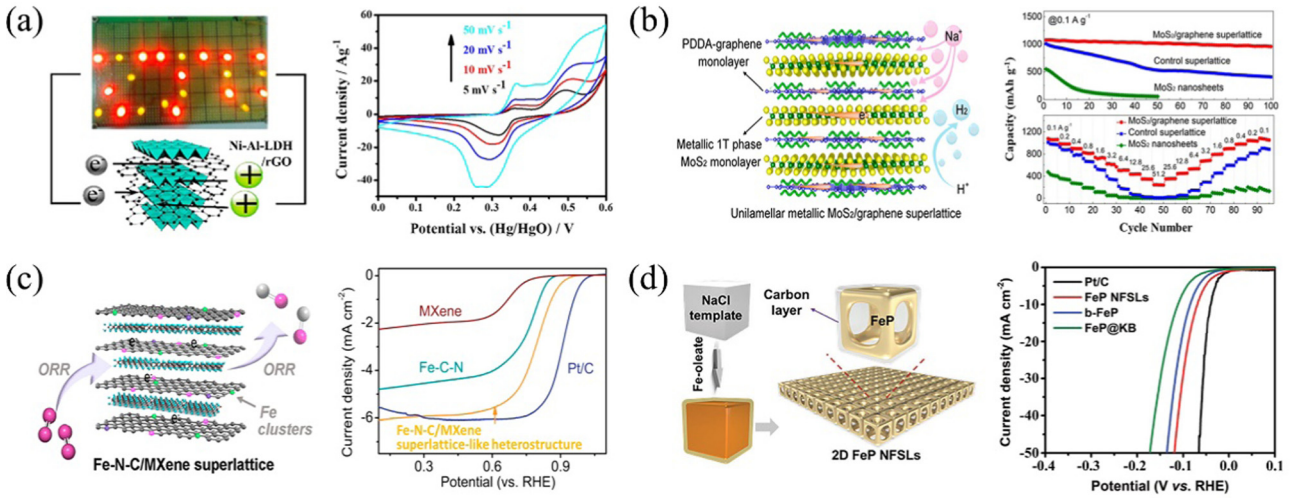

Fig. 4 (a) Schematic and cyclic voltammetry (CV) curves of a Ni–Al LDH/rGO CS supercapacitor. Reproduced with permission.[95] (b) Schematic of effective sodium storage and hydrogen release through MoS_2/graphene CSs. Reproduced with permission.[96] (c) Fe-N-C/MXene CS and its electrochemial oxygen reduction reaction plots. Reproduced with permission.[97] (d) Preparation process and hydrogen evolution reaction characterization of a 2D FeP nanoframe superlattice. Reproduced with permission.[49] Copyright 2016, Elsevier. Copyright 2018, 2020, American Chemical Society. Copyright 2022, Wiley-VCH.

a high-performance anode material for Na ion storage. The relevant battery maintained an ultralong cycle life at a high current density and a low temperature of −5 °C.[108] The graphene/MoS_2 CSs exhibited ultrahigh performance as anodes for Na-ion batteries (Fig. 4b), while the SnO/graphene CSs provided Li-ion storage with excellent cycling stability.[96]

In addition, CSs are also applied to improve the catalytic performance by controlling their electronic motions.[109,110] Compared with the bulks, CSs formed by ordered-stacked nanosheets can provide more available active sites and thus exhibit stronger catalytic properties. In 2020, Jiang *et al.* proposed a metal cluster function in preparing Fe-N-C-/MXene CSs.[97] Metal clusters were used to regulate the surface charge of nanosheets, which proves excellent electrocatalytic oxygen reduction reactions (Fig. 4c). Recently, another hydrogen evolution experiment using FeP nanoframe CSs has drawn people's attention.[49] Due to unique topochemical transformation processes, the higher efficient and durable electrocatalysts were obtained here compared with the performance of most previous FeP-based catalysts (Fig. 4d). The development of 2DSs provides new opportunities for the design of new advanced materials and catalysts.[111]

3.1.2 Quantum tunnelling and optoelectronic device. Light emission is a typical application of superlattices with the help of quantum tunnelling behavior of carriers,[1,2] so people's initial desire for preparing CSs is to study their luminescence properties.[39] Compared with traditional 2D materials, the CSs have better properties in carrier mobility and recombination probability. Together influenced by the higher efficiency of photogenerated carrier injection, the related light-emitting devices have better optoelectronic performance in response rate, luminous stability and other aspects.

In 2015, Novoselov *et al.* designed a CS made of few-layered graphene, TMDs and h-BN materials.[33] The graphene acted as conductive layers, injecting electrons and holes into the TMDs. The h-BN materials were tunnel barriers (TBs), forming quantum wells (QWs) together with the TMDs on the side. By superimposing QWs and fine controlling over the tunnelling barriers, the carrier's chances of escape are greatly reduced, increasing the luminous efficiency greatly. Here, the quantum efficiency of related devices was ∼8% (Fig. 5a). Similarly, in 2019, Gu *et al.* combined a h-BN/WS_2 CS with a distributed Bragg reflector (DBR) and invested the exciton–polariton electroluminescence (EL) at room temperature (Fig. 5b).[112] Due to the strong coupling between CSs and DBR, the external quantum efficiency (EQE) can reach ∼0.1%. In 2020, Lee *et al.* proposed a coupled QW stacked with alternating h-BN and WS_2 to observe its photoluminescence (PL) phenomenon. The h-BN retained interwell interactions dramatically, increasing the exciton energies in quantum traps. Correspondingly, the PL peaks appeared and enhanced linearly with the increase of QW periods.[113] In 2021, Kumar *et al.* also designed CSs composed of periodic TMD/h-BN/Al_2O_3 materials.[114] The luminescence intensity and efficiency were significantly changed by tuning the period number and power of excitation light (Fig. 5c). Notably, although the strong exciton properties of TMDs mentioned above are beneficial to luminescence, the relative low efficiency still poses a challenge to their practical applications. In contrast, perovskite materials present greater advantages. In 2016, Wang *et al.* developed a solution-processed perovskite light-emitting diode and achieved an EQE of 11.7% (Fig. 5d).[115] The performances of devices remained more than 82% after unpackaged even they were placed in an atmosphere with 40% humidity for 2400 h.

In addition, the above quantum tunneling of carriers between barriers can also give rise to exotic properties of materials such as the negative differential resistance (NDR) phenomenon.[116] In conventional type III heterostructures, a

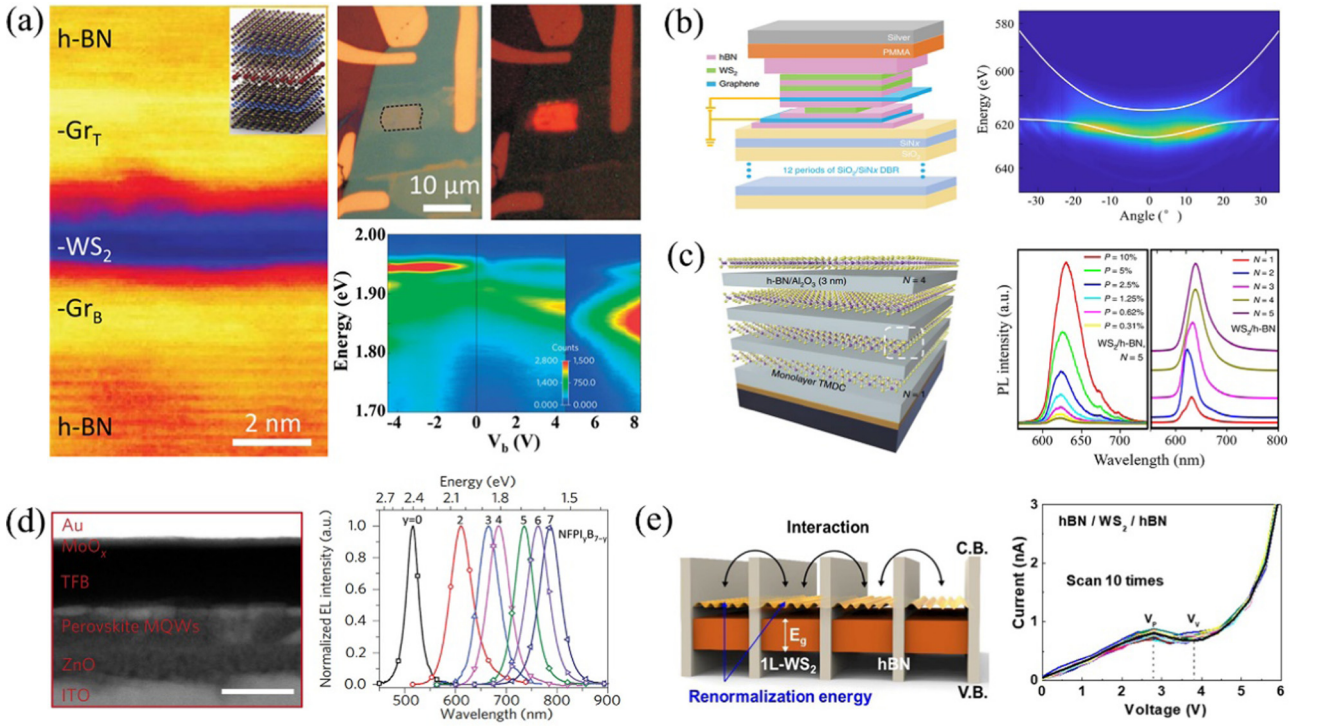

Fig. 5 (a) TEM (left), optical and EL (top) images of a CS sample. Maps of PL and EL spectra of the related devices (down). Reproduced with permission.[33] (b) Structural schematic and angle-resolved PL properties of a luminescent device integrated a h-BN/WS_2 CS with a distributed Bragg reflector. Reproduced with permission.[112] (c) Structure and PL characterizations of a TMD/h-BN/Al_2O_3 multiple QWs CS sample. Reproduced with permission.[114] (d) TEM image and EL spectra of a layered perovskite-based light-emitting diode. The scale bar is 50 nm. Reproduced with permission.[115] (e) Electronic band structures and NDR behaviors of a h-BN/WS_2 CS device. Reproduced with permission.[113] Copyright 2015, 2016, 2019, 2021, Nature Publishing Group. Copyright 2020, American Chemical Society.

weak electric field drives carriers tunneling from the maximum valence band (VB) of one material with lower energy to minimum conduction band (CB) of another with higher energy. But when the bands with lower energy move up under an increased field, carrier transportation will be hindered, manifested as the tunneling current of the device decreases. This downward trend does not continue until the current rises when the new bands are matched by continuous excitation of the external electric field. As a whole, the current of the device will experience a period of decline in the process of overall increase. If the heterostructure is replaced with a superlattice with multiple QWs, this NDR phenomenon can occur many times.[117,118] The influence of this band alignment is more significant in CSs due to the sharper interface between layers, so a more obvious NDR behavior was predicted in 2014.[119] The corresponding experimental phenomenon has also been observed by Lee *et al.* in WS_2/h-BN CSs in 2020 (Fig. 5e).[113]

3.1.3 Interfacial effect and superconductivity. As for the CSs constructed in a periodic out-of-plane stacking architecture, they have abundant interfaces and can be convenient for electron interactions. The electrons correlate strongly together influenced by the quantum confinement effect, and the charge, spin, orbit and lattice are coupled simultaneously, inducing phase transitions in CSs exhibited as novel physical phenomena such as superconductivity.[120] For example, in 2020, Checkelsky's group prepared Ba_3NbS_5/H-NbS_2 CSs for the first time (Fig. 6a).[121] Due to the inversion symmetry breaking, a mixed spin-orbit texture on the H-NbS_2 layers was obtained, which results in a Berezinskii–Kosterlitz–Thouless (BKT) transition of this architecture at about 0.82 K. In another work, Li *et al.* also observed the coexistence of superconductivity and ferromagnetism in $SnSe_2$/$Co(Cp)_2$ CSs.122 Normally, the above two phenomena are exclusive with each other because of the contradictorily ordered Cooper pairs. But here, by constructing a superlattice, a good amount of electrons in $Co(Cp)_2$ were injected into $SnSe_2$, resulting in an increase in the density of states (DOS) near the Fermi surface and triggering a semiconductor to superconductor transition. This process weakens the coordination field of $Co(Cp)_2$ and leads to its high spin state with ferromagnetic behaviors (Fig. 6b). It can be seen that the huge contact area, strong interfacial coupling effect and prominent electron-giving and electron-receiving ability of different components in CS materials are the main reasons for triggering the transition at low temperatures. Thereafter, Li *et al.* demonstrated a similar phenomenon in another TaS_2 molecular CSs.[123] Due to the strong spin-orbital scattering, a superconductivity transition could be observed at ~3.8 K (Fig. 6c).

3.2 Properties and applications of SS

The properties of CSs, especially in the field of optoelectronics, are mainly attributed to their periodic modulation of band

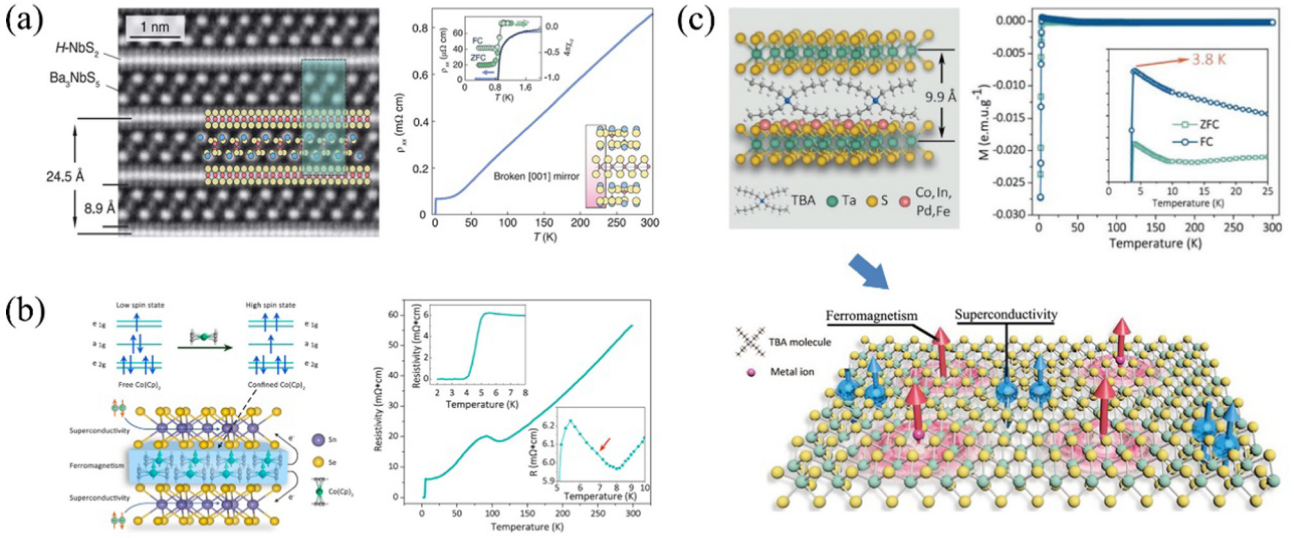

Fig. 6 (a and b) Schematic and temperature-dependent resistivity of a H-NbS_2/Ba_3NbS_5 ($SnSe_2$/$Co(Cp)_2$) superlattice. The devices exhibit the superconducting transition at temperatures below 0.8 and 4 K, respectively. Reproduced with permission.[121,122] (c) Temperature-dependent resistivity of a Co-TaS_2 molecular superlattice. Interestingly, the device exhibits ferromagnetism under field-cooling and zero-field-cooling processes. Reproduced with permission from.[123] Copyright 2020, American Association for the Advancement of Science. Copyright 2017, American Chemical Society. Copyright 2020, Wiley-VCH.

structures, but the complex preparation process always limits the further development. So, it is natural to think of other methods to achieve the modulation, gradually leading to other types such as SSs. 2D materials possess a high Young's modulus and usually exhibit stronger mechanical strength than their bulk materials.[124] By inducing strain or other factors to change the band structures, the interfacial performance of 2D materials can be tailored effectively. When introducing the modulation periodically at the nanoscale, the carrier transportation will be greatly altered, causing behaviors like conventional superlattices.[8–11,125,126] This is one of the main bases to judge whether the material studied is SS. Due to an emerging material system in almost the last 5 years, most related works are still focused on the properties exploration now.

In 2017, Andrei's group reported a feasible route to introduce a pseudomagnetic field to graphene by inducing periodic strain.[57] The band structure of graphene was reconstructed into pseudo-Landau levels (PLL) and a sequence of PLL peaks in the DOS were observed (Fig. 7a). The similar phenomenon was reported again in 2019.[26] Interestingly, this time they presented a new way for making flat bands in another graphene SS, which is expected to be a theoretical basis for the important role of this SS in superconductivity. Almost at the same time, Banerjee *et al.* also reported an intense pseudogauge field generated in a graphene SS.[77] The carbon–carbon bond length changed and affected Dirac electrons. The DOS fluctuates periodically with an applied bias, and the period is directly related to the spatial scale of the periodic strain in SS (Fig. 7b). In addition to the above research, the quantum confinement enhancement and periodic energy valley properties are involved recently, which also predicts the prospect of SS applied in the photovoltaic fields.[127,128] In 2020, Tian's group investigated the difference of interfacial interaction between the pristine graphene and SS (Fig. 7c).[129] Compared with the relatively low photocurrent value in the central region of the superlattice, the photocurrent increased significantly at the interface between original graphene and SS. By analyzing the photothermoelectric current (I_{PTE}) formula $I_{PTE} = \Delta S \cdot \Delta T/R$, where ΔS, ΔT and R are respectively the Seebeck coefficient difference between the two regions, temperature difference around the light point and device resistance, they concluded that the large Seebeck coefficient shift caused by the deformation of the internal band structure plays a key role here.

Apart from the periodic strain, introducing the external localized fields can also modulate the performance of 2DSs.[130,131] By transferring a 2D material onto a substrate with periodic nano-structures as the design, the material may behave as a superlattice. In this sense, the definition of above-mentioned SS can be further extended. For example, in 2018 Chen *et al.* applied an out-of-plane periodic electric field on the silicene and observed the typical NDR behaviors usually presented in CSs (Fig. 7d).[132] Interestingly, the devices exhibit controllable valley and spin degrees of freedom for modulation, suggesting a broader application prospect. In another work, Forsythe *et al.* transferred an h-BN/graphene/h-BN heterostructure onto a SiO_2 substrate with periodic triangular/square nanohole arrays.[27] When the material was stimulated by a magnetic field, the fractal mini-gaps of the Hofstadter spectrum were observed (Fig. 7e). The quantum Hall effect is completely caused and amplified by the band structure modification arising from the substrate. The intensity of the magnetic field that needs to be applied here is nearly an order of magnitude lower than that in most MSs.[133,134] Similarly, by designing an h-BN/graphene/h-BN heterostructure etched with periodic nanoholes, Jessen *et al.* also

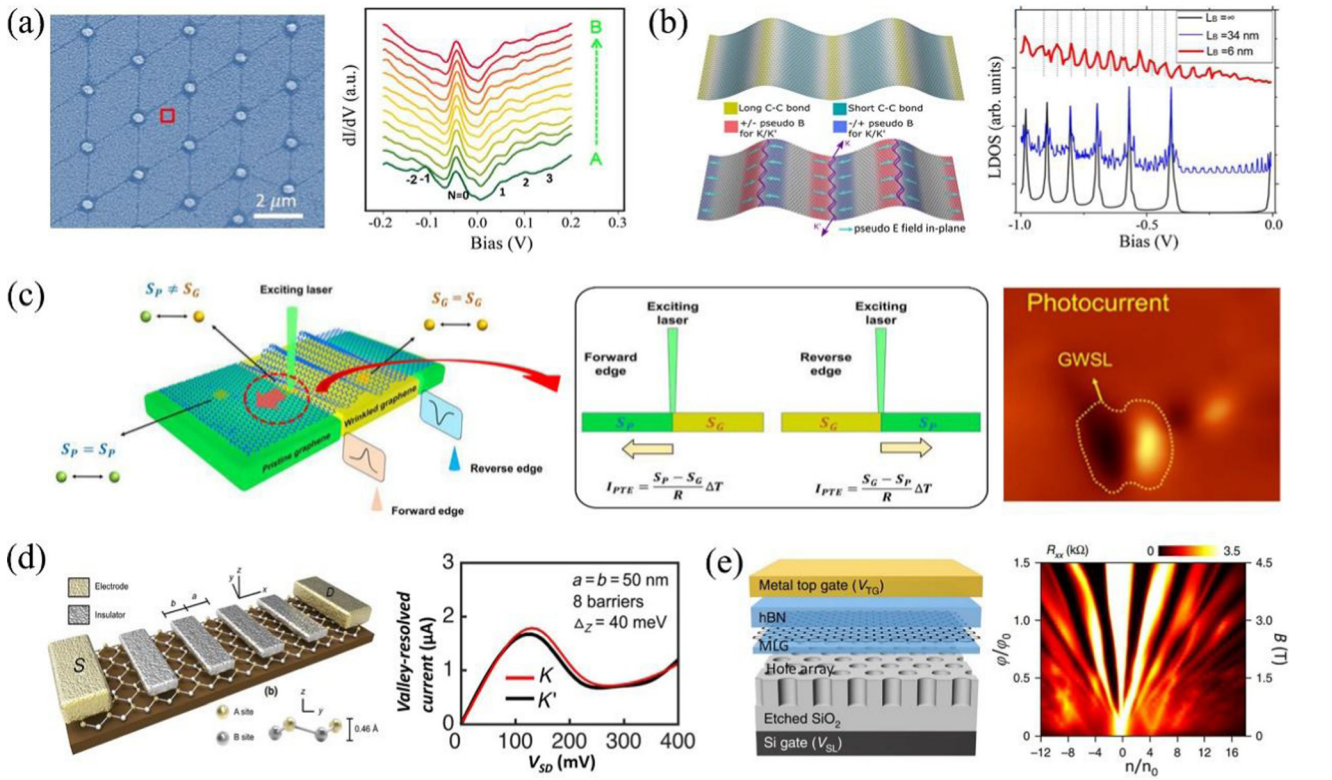

Fig. 7 (a) Left: SEM image of a graphene/Au pillars SS sample. The periodic dots and dark lines are Au pillars and strain-induced graphene ripples, respectively. Right: Spatial-dependent dI/dV curves of the SS sample. Different from the featureless 'V' shape of unstrained graphene, the SS graphene sample exhibits many peaks here, indicating the presence of pseudomagnetic field. Reproduced with permission.[57] (b) Pseudogauge fields and calculated DOS of a graphene SS. When the strain period applied to the material changes, the energy peak period of Landau quantization changes accordingly. Reproduced with permission.[77] (c) Schematic and enhanced photocurrent of a graphene SS. The difference in Seebeck coefficients between the pristine and folded graphene enhances the photothermoelectric effect at the interface. Reproduced with permission.[129] (d) Structural schematic and NDR behaviors of a silicene SS. Reproduced with permission.[132] (e) Schematic and longitudinal resistances at different normalized densities and magnetic fields of a graphene/dielectric hole SS. Reproduced with permission.[27] Copyright 2017, 2020, American Chemical Society. Copyright 2018, American Physical Society. Copyright 2018, Nature Publishing Group.

modulated the band structure of graphene.[28] In 2021, by placing graphene/h-BN on SiO_2 nanoarray structures, Dean *et al.* synthesized another SS and observed the main and satellite Dirac cones later.[135]

In addition to the above reports that 2DSs can be achieved by an applied field, considerable recent work has focused on conducting periodic nanomachining on 2DCSs to directly regulate their properties. For example, a CS prepared with periodic stacking of graphene and dielectric films has been reported as a hyperbolic metamaterial, and it absorbs an incident electromagnetic wave perfectly in the near-infrared (NIR) band.[136] By preparing a nanograting on its surface, the absorption can be further extended to the visible range. In another work, Yan *et al.* periodically arranged graphene with an organic buffer layer and etched it into ribbons and discs. After the treatment, the materials can modulate the plasmon in graphene and respond to polarization or strongly absorb terahertz or far-infrared waves.[137] In this case, the 2DSs and metamaterials have many similarities in their properties. A clearer definition is needed in the future to distinguish between the two.

Apart from the above discussion, there are still several points to note about SSs. First, due to the high Young's modulus, the deformation of 2D materials under the action of vdW forces between the interfaces is inevitable when transferring them onto other 2D materials or substrates. Once the strain exceeds a critical value, the periodic interfacial buckling will appear and the changes in material properties cannot be ignored. This is the reason why people hope to regulate the properties of 2D materials by constructing SSs. Second, regulating the band structures of original materials for tuning their properties is still dominant in most of the existing SSs. But because the specific physical mechanisms involved are different, it is hard to describe the strain in the superlattice quantificationally. At the same time, considering the different natures of materials itself and the forms of strain, it is also difficult to establish an accurate correspondence between strain and the related properties/applications. Finally, whether the strain plays a major role in the process of material property changes needs a comprehensive consideration. Multiple forms of interactions are observed simultaneously in a certain class of superlattices, and they may work together to cause a particular

property of the material. This is also one of the main reasons it is hard to quantificationally evaluate the influence of strain. However, in-depth research in this area will require a great deal of work to be done.

3.3 Properties and applications of MS

From the perspective of the development of 2DSs, the research of MSs does not show obvious lag compared with others.[138] However, it is indeed the research on superconductivity and Mott-like insulating properties reported on TBG that has attracted more attention.[21,22] Up to now, the components of designed MSs have been extended from different 2D materials to others such as photonic crystals.[139] An emerging 'twistronics' involving the studies of light spin/valleytronics, localization/delocalization phenomena, topological exciton bands, *etc.* are developing vigorously.[30–32,140–142] Since this field is in its initial development stage, most of the research on MSs is still in the performance exploration. To be different from the existing review work, here the complex theoretical descriptions are avoided and the introduction of the material properties and related practical applications are mainly focused on.

3.3.1 Electrical properties and related devices. In 2018, Cao *et al.* observed the superconductivity and Mott-like insulating properties in TBG at low temperatures (<1.7 K) for the first time.[21,22] When the upper and lower layers of graphene are rotated relatively at small angles to each other (magic angles, MAs), the bands near the Fermi energy of the whole material system will become flat (Fig. 8a). The effective masses of carriers rise high and the Fermi velocities drop to zero. The original weakly correlated Fermi liquid transforms to a strongly correlated 2D electron system, which is demonstrated again with the Fourier transform photocurrent spectroscopy recently.[143] From the phase diagram in Fig. 8a, both the insulating and superconducting phases in TBG can be observed. The occurrence of each condition just depends on the electrons filling state per unit cell. Similar results were also reported in a 0.93° TBG-MS.[144] These works attracted attention and propelled people to do more research on the related MSs.[145–148] For example, Cao *et al.* further studied the

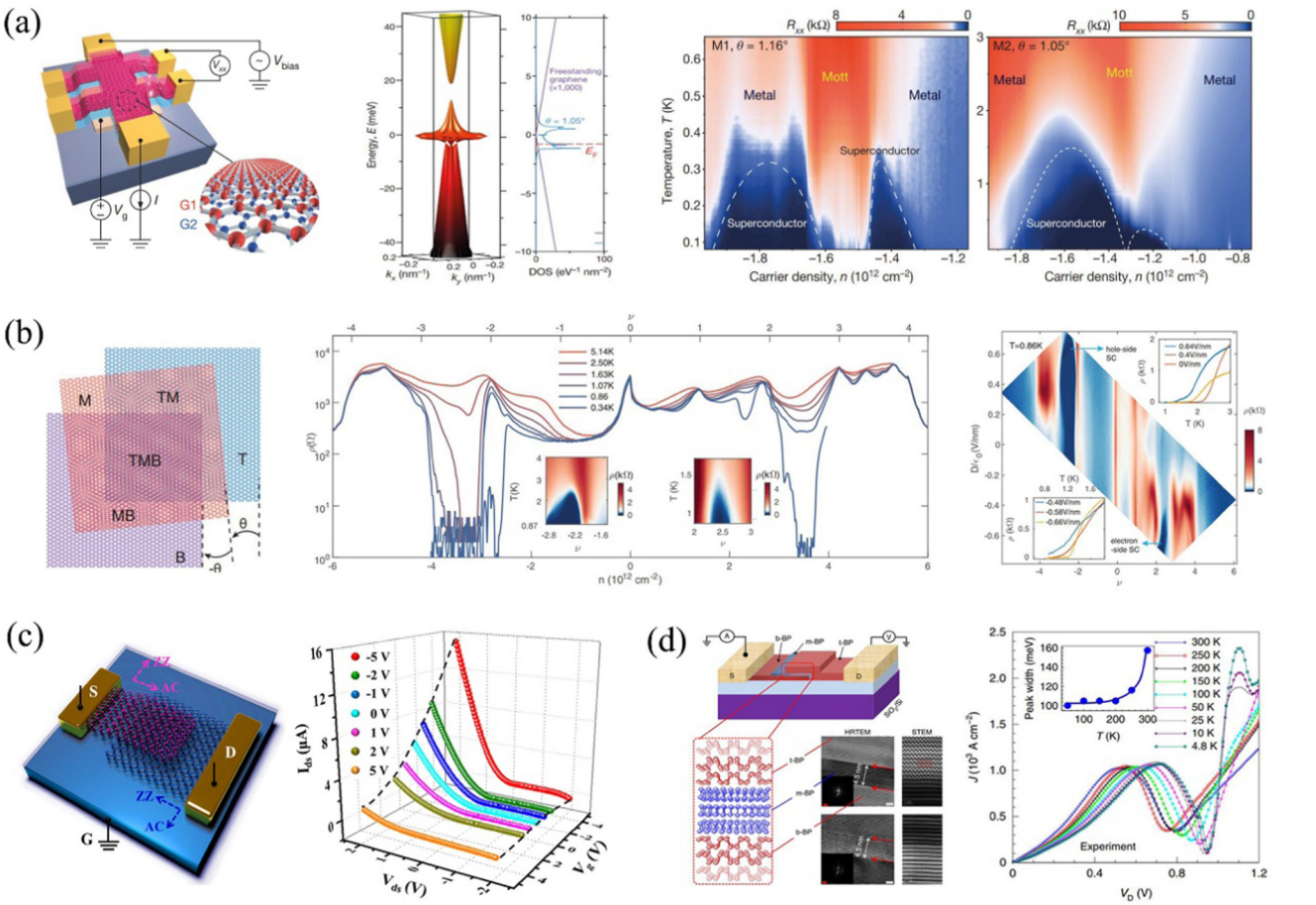

Fig. 8 (a) Schematic (left), energy band structure, DOS (middle) and temperature-dependent four-probe resistances (right) of different TBG-MS samples. Two superconducting domes are observed. Reproduced with permission.[21] (b) Schematic (left), temperature-dependent resistances (middle) and resistance map (right) with different Landau fans and applied displacement fields of a TTG-MS sample. Reproduced with permission.[148] (c) Schematic and rectified electrical properties of a BP orientation-dependent photodiode. Reproduced with permission.[149] (d) Schematic, TEM images and temperature-dependent NDR behaviors of a trilayer orthogonal BP MS. Reproduced with permission.[151] Copyright 2018, 2021, Nature Publishing Group. Copyright 2018, Wiley-VCH. Copyright 2021, American Association for the Advancement of Science.

properties of a twisted bilayer–bilayer graphene (TBBG) in 2020.[145] The richer phase diagrams and more sensitive correlated insulating states to environments were observed. In 2021, they prepared a magic-angle twisted trilayer graphene (TTG) and proclaimed a system with more controllable properties.[146] The broken-symmetry phase per unit cell was the forming reason. Based on the subsequent observations of re-entrant superconductivity at large magnetic fields (>5 T), they believed that a mechanism resulting in non-spin-singlet Cooper pairs plays a key role.[147] Almost at the same time, Kim's group did a similar experiment in a 1.56° TTG.[148] Compared with TBG, the superconductivity here was more robust and the maximum critical temperature rose higher at $\sim$2.1 K. By changing the integer fillings, temperatures and displacement field intensities, the superconductivity phases can be tuned accordingly (Fig. 8b).

The flat band properties in TBG or TTG have promoted the rapid development of similar systems, but their practical applications in electronics are still rare.[31,139] People are trying to do research from the perspectives by considering different materials and device structures. In 2018, Xin *et al.* fabricated the orientation-dependent diodes by observing the rectification in few-layered BP vdW MSs.[149] The armchair (AC) orientation of the upper BP is vertical to the lower one (vertical-twisted BP), and maximum rectification ratio of the diode reaches 115 (Fig. 8c). In contrast, the devices made of 'parallel-twisted BP' show completely different linear ohmic behaviours.[149,150] The anisotropic band structure of BP and the discrepant effective mass of electrons and holes are the main reasons for this phenomenon. Based on the formula $\Delta E = k_B T \cdot \ln(m^*_{AC}/m^*_{zz})$, where k_B, T and m are the Boltzman's constant, kelvin temperature and effective mass of carriers respectively, the band difference (ΔE) between the armchair (AC) and zigzag (ZZ) orientations could be estimated. Similar results were also found by Lee's group in 2021, but the difference was the observation of a symmetric nonlinear voltage–current curve instead of the rectification phenomenon.[151] This may be related to the oxidation protection on BP in the former experiment. By fabricating more complex BP-MS structures, Lee *et al.* further prepared the resonant tunnelling diode, which exhibits a typical NDR phenomenon (Fig. 8d). In order to explore the mechanism, a physical model described by two-band block Hamiltonians was established. They believed that the different crystalline orientations between adjacent BPs lead to the changes of band structures, so that the QW states originate from the electronic wavefunction confinement appeared, resulting in the resonant tunnelling behaviors similar to that in traditional superlattices. Significantly, the BP MSs here present great advantages in modulating and optimizing the performance of related devices in normal environment. This is different from the TBG systems in that their flat band properties are usually observed at low temperatures.

3.3.2 Optical properties and related devices. Compared with the electrical properties, the optical properties of MSs are studied earlier in experiment due to the more predictable mechanism and simpler preparation of samples. For instance, in early 2009, Andrei's group has observed the Van Hove singularities (VHSs) in the density of states in TBG by using scanning tunnelling spectroscopy. By changing the rotation angles between the stacked graphene layers, the positions of VHSs change gradually regardless of the lattice commensurability.[38] In 2013, Moon *et al.* theoretically predicted the relationship between rotation angles and VHSs.[152] The exceptional characteristic has a great influence on the optical properties of TBG especially for its optical conductivity values, which causes the sample at a certain twisted angle to have an unusual response to incident light with a particular wavelength. This conclusion is verified in the enhanced photo-absorption, Raman spectroscopy and second/higher harmonic generation measurements, *et al.*[152–156] For example, in 2012, Kim *et al.* obtained the relationship between the incident light and Raman vibration intensity of TBG with different twist angles (θ_c).[154] $\theta_c = 3a \cdot E_{laser}/\hbar \cdot \nu_f \cdot 4\pi$, where a, E_{laser}, $\hbar$ and ν_f are the lattice parameter of graphene, Raman excitation laser energy, reduced Planck's constant and Fermi velocity in monolayer graphene, respectively. Through the formula, we can simply establish the relationship between the interlayer twist angle and the wavelength with an enhanced photoresponse. In 2021, Ha *et al.* further explored the third harmonic generation (THG) in the same system.[156] When the energy band gap at the VHSs matches the three-photon resonance of incident light well, the THG efficiency is found to be greatly improved by up to 60 times compared with the normal monolayer graphene (Fig. 9a).

With the deepening research in recent years, the optical properties exploration of MSs has been expanded in a large range, such as in the field of optical coherent injection, chiral circular dichroism, light-induced ferromagnetism and so on.[157–159] The different material systems have also attracted constant attention. For example, in 2020, Qiu's group predicted that the photonic dispersion of phonon polaritons in twisted α-MoO_3 can transition topologically from hyperbolic to elliptical contours with changing the sample angle.[160] Under a particular rotation (photonic MA), the dispersion flattens and causes diffractionless polariton propagation. This expectation was confirmed in the experiment afterwards and the light wavelength was compressed 40 times in this method, suggesting an important development prospect in nanoimaging or other fields (Fig. 9b). Similar results were also confirmed by Chen *et al.* subsequently.[161]

Apart from the optical research mentioned above, the PL of MSs is also an engrossing field which is closest to practical applications at present. Different from the zero bandgap of graphene material, TMDs or photonic crystals have a greater advantage in light emission due to its sizeable bandgap. In 2014, Liu *et al.* studied the luminescence properties of MoS_2-MSs and discussed the interlayer exciton coupling by observing the variation of spectral peaks.[68] Subsequently, various groups studied in detail the relationship between PL and twisted angle of different TMD-based MSs, respectively.[162–164] Due to the momentum mismatches and formation of resonance hybridized excitons during rotation, the twisted angle can still lead to a huge difference in the luminescence

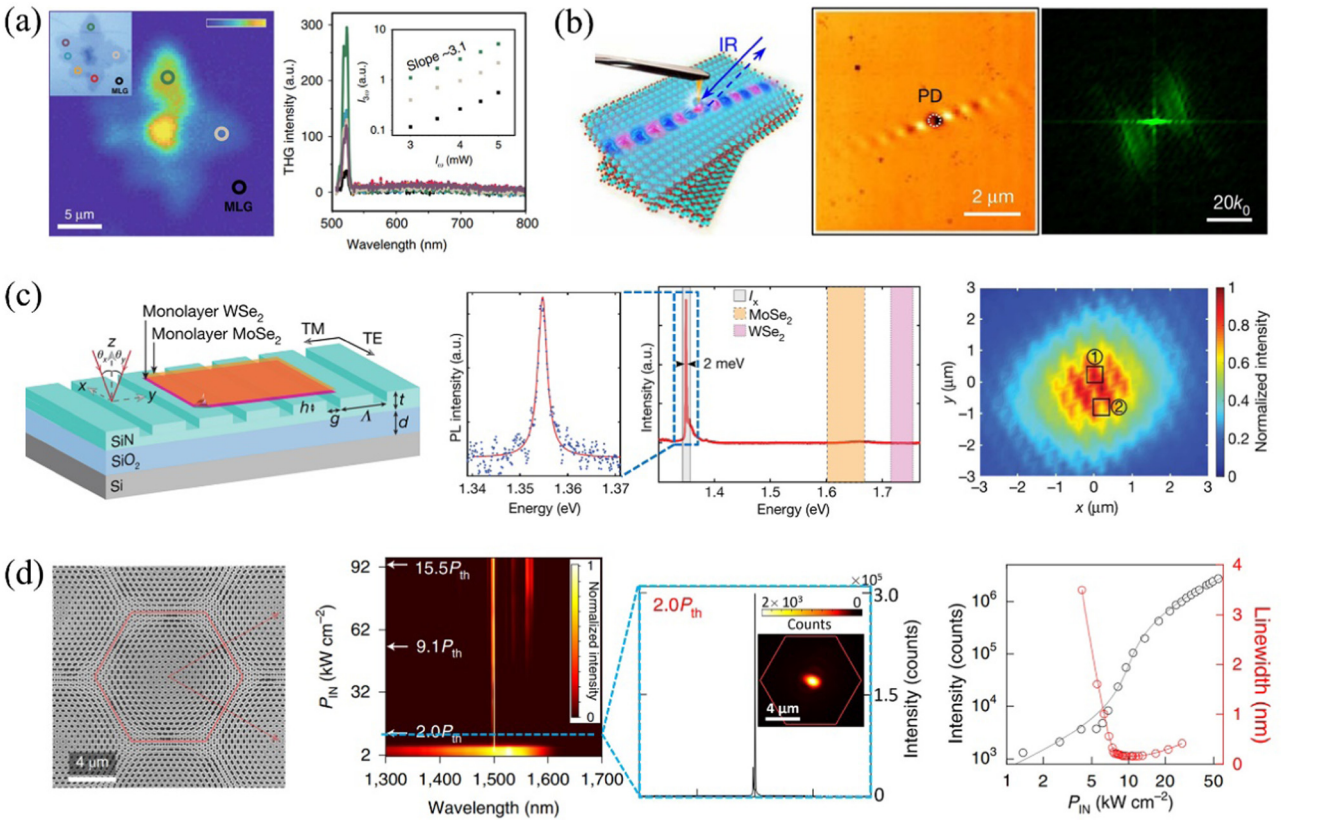

Fig. 9 (a) Left: Scanning THG image of a graphene sample with uneven thicknesses. Right: Typical THG spectra of the graphene sample at different regions excited by 520 nm laser. The TBG position can be excited by the strongest signal. Reproduced with permission.[156] (b) Schematic (left), near-field amplitude distribution (middle) and its Fourier transformed dispersion curves of a twisted α-MoO_3 sample. A highly oriented amplitude distribution in the middle indicates anisotropic topological polariton transportation. Reproduced with permission.[160] (c) Schematic (left), PL spectrum (middle) and a typical interferograms (right) above threshold of a 0°-twisted WSe_2–$MoSe_2$ exciton laser. Reproduced with permission.[170] (d) SEM image (left), normalized spectra (middle) and intensity/linewidth evolution curves of a nanostructured magic-angle laser on InGaAsP multiple QWs. A phase transition from spontaneous emission to laser above threshold can be found from the normalized spectra. Reproduced with permission.[171] Copyright 2019, 2020, 2021, Nature Publishing Group.

properties even if the material remains unchanged. Although the mechanism of the TMD-based MSs is still controversial, the spin-valley locking effect and controllable moiré exciton properties in electromagnetic fields also lay a solid foundation for their practical applications.[165–169] In 2019, Paik *et al.* integrated a WSe_2–$MoSe_2$ bilayer material with a silicon nitride grating resonator.[170] By accurately matching the momentum of the TMD-MS and stimulating the interlayer excitons, they achieved a more than 100-fold increase in light emission across the lasing threshold (Fig. 9c). An extended spatial coherence length proves laser generation rather than ordinary luminescence. In 2021, Ma's group further introduced the concept of MSs into photonic crystals and fabricated the samples which contains two in-plane sets of nanohole arrays with a twisted angle in a single InGaAsP material.[171] Due to the stronger field confinement, the devices made of these nanocavities can emit lasers with a narrower spectral linewidth (Fig. 9d).

3.3.3 Photoelectronic properties and photodetectors. The photoelectric properties of MSs correlate the electrical and optical behavior of related devices, focusing on their conversion of optoelectronic signals. Although the MSs have shown great potentials in solar energy harvesting, electroluminescence and so on, the photodetection is still the most practical in this field.[172,173] In 2016, due to the twist-angle-dependent VHSs of TBG, Liu's group observed the enhanced photoresponse related to the wavelength of incident light in this system for the first time.[153] By integrating the TBG with plasmonic nanostructures, they achieved up to an 80-fold increase in photocurrent. Almost at the same time, Tian's group observed similar phenomena and described in detail the polarization-dependent characteristics of related devices (Fig. 10a).[61,174] Subsequently, by effectively collecting multiple hot carriers in graphene/h-BN MSs photodetectors, Wu *et al.* also enhanced the photocurrent and improved the EQE of graphene.[175] Notably, most of the response bands of the above devices are focused on the visible range, and the twisted angles are relatively large. By contrast, if the rotation of MS is limited around the 'MA', the transition of carriers between mini-bands available during energy band variation will cause the material to respond to electromagnetic waves with longer wavelengths. Guided by this idea, in 2019 Xia's group designed a TBG photodetector with 1.81° twisted angle and measured the photoresponse in the

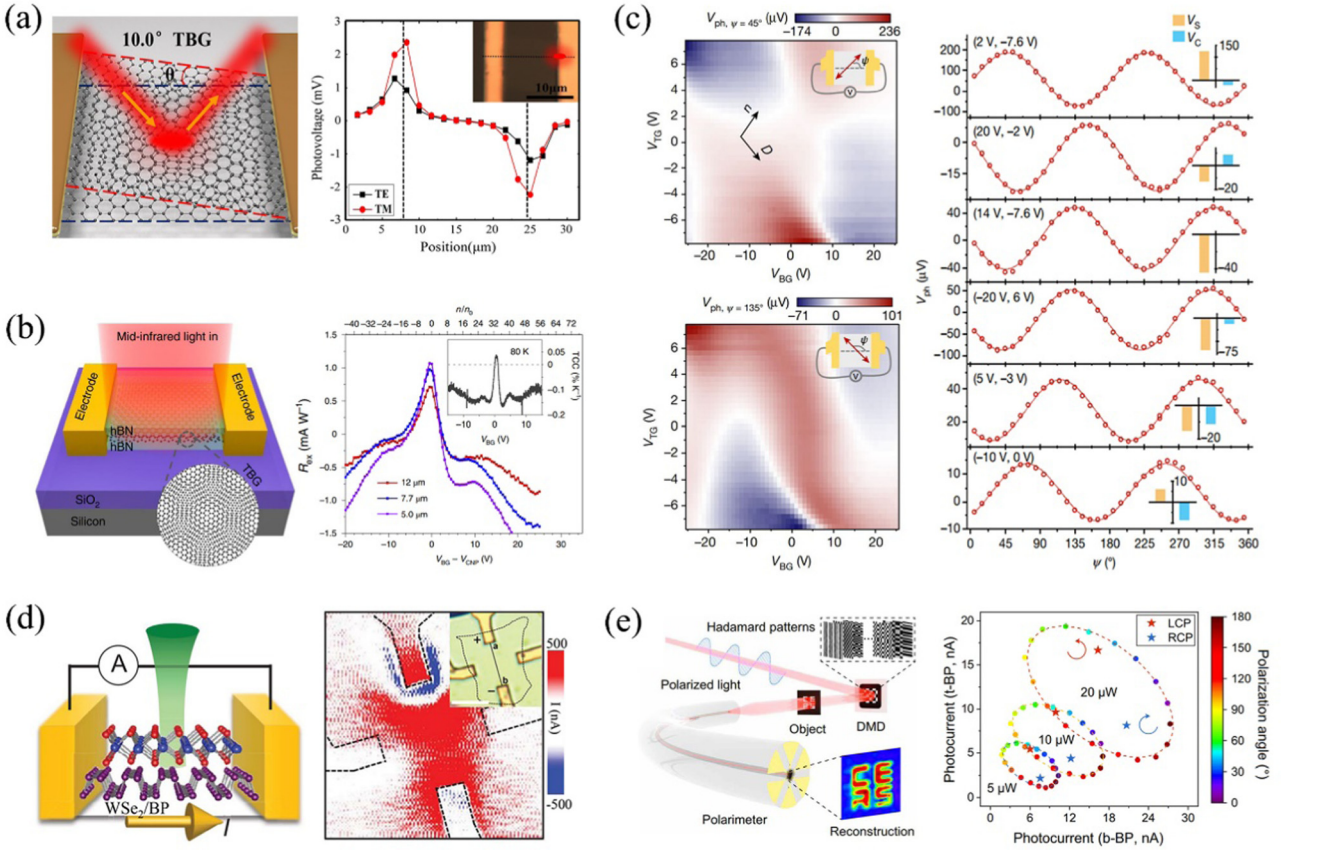

Fig. 10 (a and b) Schematics and photoresponse measurements of TBG MSs in visible and mid-infrared bands respectively. Reproduced with permission.[174,176] (c) Left: Gate-tunable linear bulk photovoltaic voltage (V_{ph}) excited by a linearly polarized light (λ = 7.7 μm) with polarization angle ψ = 45° (top) and ψ = 135° (bottom), respectively. Right: Polarization dependence of V_{ph} when fixing the gate voltages. Reproduced with permission.[177] (d) Schematic and photocurrent mapping of a WSe2/BP photodetector excited by a linearly polarized 532 nm laser. Reproduced with permission.[179] (e) Schematic and 2D polarization-dependent photocurrent of a twisted BP/BP/Bi_2Se_3 fiber-integrated polarimeter. Reproduced with permission.[180] Copyright 2016, Wiley-VCH. Copyright 2021, 2022, American Association for the Advancement of Science. Copyright 2020, 2022, Nature Publishing Group.

mid-infrared range.[176] By gate-tuning the Fermi level in TBG to the bandgap, the device can achieve a maximum photoresponsivity of 26 mA W^{-1} at 12 μm (Fig. 10b). Recently, by breaking the symmetry and introducing quantum geometric contribution to graphene through moiré deformation, they further observed the bulk photovoltaic effect (BPE) in 1.2° TBG samples at 5 and 7.7 μm wavelengths, relating the BPE to the anisotropic conductivity by the following equation: $V \propto E\,(\sigma_{xxx}\cdot\cos(2\varphi) - \sigma_{yyy}\cdot\sin(2\varphi))$, where φ is the orientation angle of the in-plane field E with respect to the voltage collection direction (x axis). Since the photoresponse of TBG is directly related to incident light intensity and polarization here, the related devices achieved the full-Stokes polarimetry and presented a great development prospect in on-chip photodetection (Fig. 10c).[177] Combined with the heat capacity influence of this material system, it is expected to further expand the detection wavelength and improve the detectivity.[178]

In addition to the graphene-based MS mentioned above, recently the MS made of other 2D materials have also attracted extensive attention in photodetection. In 2021, Akamatsu *et al.* designed a WSe_2–BP MS and observed its spontaneous photocurrent without actuation by a bias voltage.[179] Different from the traditional heterostructures, the strict crystal alignment needs to be considered. Only when the threefold rotational symmetry of WS_2 is parallel to the AC direction of BP, the interesting phenomenon can occur. From the photocurrent map we can find that the photoresponse appears in the stacking area instead of the material–electrode junction (Fig. 10d). This is similar to that in the BP homostructures, and the geometrical and topological nature at the WSe_2–BP interface play a key role.[150] In another work, Xiong *et al.* integrated a few-layered Bi_2Se_3-BP-BP MS into the end face of a fiber to measure the intensity and polarization of incident light rigorously (Fig. 10e).[180] They established the following relationship between photocurrent (I), light power (P) and polarization angle (φ):

$$I = m\cdot P^n,$$

$I = I_C\cdot\sin(2\varphi) + I_L\cdot\sin(4\varphi + \varphi_0) + I_0$, where m and n are fitting coefficients, and φ, φ_o and I_0 are the polarized angle, initial polarized angle and light power, respectively. The in-plane anisotropic properties of BP and ingenious geometric structure of devices are mainly considered. Based on the above formulas,

the detector here can detect both the intensities and polarized angles of incident light, which also provides a new idea for the practical applications of MSs in polarization optics.

3.3.4 Other properties and potential applications. The magnetic response of MSs has attracted much attention recently due to their closely related quantum or topological properties.[30–32,140] Similar to other properties, the magnetic study of MSs also starts from TBG materials. The linear dispersion at low energy enables them to have strong electron–electron interactions, resulting in an arresting modulation of quasiparticles by Landau quantization in a magnetic field. The most intuitive manifestation of this quantization is the emergence of Fermi velocity renormalization and the quantum Hall phenomenon.[181–183] When the Fermi level of TBG is adjusted between two Landau levels by changing the magnetic field intensity, a platform for Hall conductivity can be observed.[184] These magnetic behaviors do not necessarily require the material to be in an external magnetic field, but can also be achieved by controlling the layer twist angle, moiré carrier filling or electrical field. For example, in 2012, Wang *et al.* theoretically predicted the existence of pseudo-Landau levels if a bias is applied to adjust the Fermi level of TBG samples to their VHS peaks.[133] Soon afterwards, Liu *et al.* tailored the pseudomagnetic fields successfully in a graphene/BP MS.[185] Recently, Xu's group further discovered that the optical excitation can also induce ferromagnetism in TMD MSs.[159] This is probably due to the exchange coupling between moiré-trapped holes interacted by the excited excitons and thus exhibiting ferromagnetic ordered behaviors. When one hole is in every three moiré unit cells, the hysteresis loops can appear in the reflective magnetic circular dichroism signal significantly (Fig. 11a).

In addition to the above magnetic novelty, MSs also present outstanding performance in mechanics and thermodynamics.[186] For example, by studying the tribological properties of h-BN/graphene MSs, Zheng's group found that lattice mismatch can lead to microscale structural superlubricity at the interface.[187] The friction changes little even in rotation of the dislocation contact and the shear stress here is about orders of magnitude lower than that in homogeneous junctions. The smooth soliton-like motion of the moiré pattern ridges was demonstrated crucial through the kinetic simulations. Not long ago, Zhang *et al.* also studied the stick slip behaviors of the same material system in detail.[188] The stick slip manifests at both the atomic and moiré scales when a nanoscale tip is slid on the h-BN/graphene MS surface (Fig. 11b). Interestingly, because the structural lubricity of the material is closely related to its thermal characteristic, the h-BN/graphene MS also provides an excellent platform for its thermodynamic study. In 2021, Ren *et al.* studied the interfacial thermal transport of this system as the twisted angle changed. This rotation caused the surface undulations between layers, enhancing the interfacial phonon scattering and influencing the thermal conductance accordingly.[189]

Besides, the interlayer coupling of carriers MSs also greatly affects the chemical reaction rate of materials. Taking the TBG material as an example, especially when the incident light energy matches well with the interval between VHSs, the chemical reactivity of graphene material will be greatly enhanced. Based on this, in 2015, Liu's group investigated the chemical reaction between TBG and benzoyl peroxide (BPO) systematically.[190] The TBG with 13° twisted angle has been shown faster chemical reaction rate (Fig. 11c). A similar phenomenon in the reactions of TBG with diazonium salts was also observed soon after by Luo's group.[191] According to

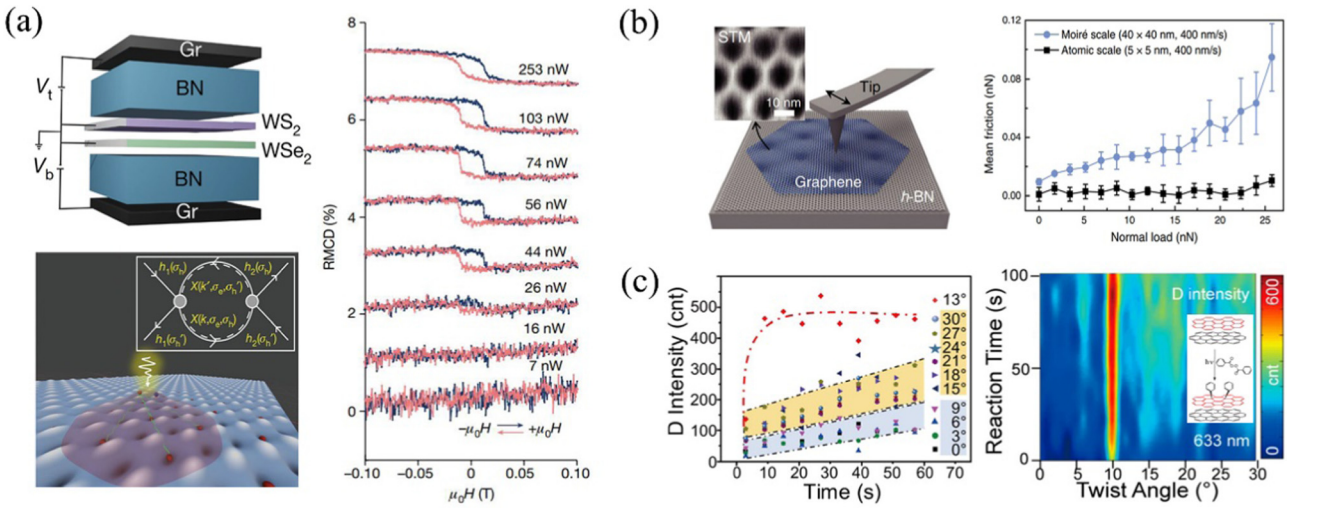

Fig. 11 (a) Schematics (left top) and optical-induced ferromagnetism phenomena (right) of a voltage-regulated WS_2/WSe_2 MS at 1.6 K. The exciton-mediated long-range spin–spin interactions play a key role here (left bottom). Reproduced with permission.[159] (b) Left: STM and schematic images of a graphene/h-BN MS. Right: The corresponding unusual stick slip measurements both at the moiré and atomic scales. Reproduced with permission.[188] (c) Comparison of chemical reactions between BPO and TBGs with different twisted angles through the Raman signatures. For some samples with specific angles, the reaction rate is enhanced. Reproduced with permission from.[190] Copyright 2022, Nature Publishing Group. Copyright 2022, American Physical Society. Copyright 2015, American Chemical Society.

Table 1 Summary of applications of 2DSs

Applications	Type	Materials	Symbolic parameters	Ref.	Year
Energy storage	CS	LDH/rGO	Capacity up to 650 F g^{-1}	40	2014
	CS	Ni-Al LDH/rGO	72.7% initial capacitance maintains after 10 000 cycles	95	2016
	CS	MoS_2/graphene	Anode delivered specific capacity of 240 mA h g^{-1} at 51.2 A g^{-1} and more than 380 mA h g^{-1} at 10 A g^{-1} over 1000 cycles, onset potential of 88 mV, Tafel slope of 48.7 mV $decade^{-1}$	96	2018
	CS	Fe-N-C/MXene	A positive onset potential of 0.92 V, strong durability of 20 h	97	2020
	CS	Co-Al LDH-NS/GO	Long cyclic life, specific capacitance up to 1204 F g^{-1} under 5 mV s^{-1}	99	2012
	CS	β-$Ni(OH)_2$/graphene	Highest specific capacitance of 660.8 F cm^{-3}	100	2013
	CS	Ti_3C_2/Ni-Co-Al-LDH	Specific capacitance of 748.2 F g^{-1} at 1 A g^{-1}, maximum energy density of 45.8 W h kg^{-1} as positive electrode	101	2017
	CS	SnO/pristine graphene	Reversible capacity of 633.9 mA h g^{-1} at 0.05 A g^{-1}, 700 cycles at 1 A g^{-1}	107	2020
	CS	CoFe-LDH/NiFe-LDH	A voltage of 1.59 V at 10 mA cm^{-2}	109	2019
	SS	$VOPO_4$-graphene	Specific capacity of 160 mA h g^{-1}, energy density of ~570 W h kg^{-1}	102	2020
	SS	WS_2 wrinkle arrays	An overpotential of 121 mV *versus* reversible hydrogen electrode	198	2021
	MS	WS_2	An overpotential of 60 mV at 10 mA cm^{-2}, Tafel slope of 40 mV $decade^{-1}$	194	2021
	MS	MoS_2	An overpotential of −153 mV at −10 mV cm^{-2}, Tafel slope of 73 mV $decade^{-1}$	195	2019
Superconductivity	CS	Ba_3NbS_5/H-NbS_2	A BKT transition at ~0.82 K	121	2020
	CS	TaS_2	A superconductivity transition at ~3.8 K	123	2020
	MS	TBG (1.1° ± 0.1°)	A superconductivity transition at ~1.7 K	21	2018
	MS	TBG (0.93° ± 0.01°)	A superconductivity transition at ~0.3 K	144	2019
	MS	TTG (~1.56°)	A superconductivity transition at ~2.1 K	148	2021
	MS	TBG (> 1.1°)	Largest superconductivity transition temperature is ~3 K with pressure	196	2019
NDR properties	CS	WSe_2/$SnSe_2$	Peak-to-valley current ratio (PVCR) of 1.8 at 300 K, PVCR of 2.8 at 80 K	116	2021
	CS	$MoTe_2$/hexacarbonitrile	PVCR of maximum ~137	199	2021
	SS	Silicene	PVCR of 4.7 under a low operating bias at room temperature	132	2018
	MS	BP	PVCR of 3 at 300 K, PVCR of ~9 at 4.8 K	151	2021
Photo absorption	CS	rGO/PDDA	Broadband absorption of >80% of unpolarized light from 300 to 2500 nm	136	2019
	SS	BP	Absorption band edge shift of up to ~0.7 eV	127	2016
	SS	MoS_2	Enhanced broadband absorption from 677 to 905 nm	201	2015
	MS	TBG (10°/13°)	~3 times the photo absorption of ordinary monolayer graphene	153	2016
	MS	Perovskite (30°)	28.5% enhancement of light harvesting	173	2021
Photodetection	SS	BP	Peak detectivity of 5.97×10^9 Jones at λ = 4.0 μm (0.4%; compressive), 8.45×10^9 Jones at λ = 2.0 μm (1.0%; tensile)	126	2021
	SS	Graphene wrinkle	Photoresponsivity of 1.8×10^{-4} A W^{-1} (> 15 times higher than pristine graphene)	129	2020
	MS	TBG	Maximum photoresponsivity of ~1 mA W^{-1} of 13.0° TBG at λ = 532 nm	72	2016
	MS	TBG	Photoresponsivity of ~9 mA W^{-1} of 10.0° TBG at λ = 633 nm	153	2016
	MS	TBG	Photovoltage of 1.2–2.2 mV of 10.0° TBG, 0.88–1.62 mV of 12.0° TBG	174	2016
	MS	Graphene/h-BN	A zero-bias photoresponsivity of 0.3 A W^{-1} at λ = 660 nm	175	2016
	MS	TBG	Photoresponsivity of 26 mA W^{-1} of 1.81° TBG at λ = 12 μm	176	2020
	MS	TBG	Response time around 4 ns, response ranges from visible to THz	178	2020
Luminescence	CS	Graphene/TMDs/h-BN	Quantum efficiency of ~8%	33	2015
	CS	h-BN/WS_2	EQE up to ~0.1%	112	2019
	CS	TMD/h-BN/Al_2O_3	>90% narrow band absorption, Rabi splitting of up to 170 meV	114	2022
	CS	Perovskite	EQE up to 11.7%, energy conversion efficiency of 5.5% at 100 mA cm^{-2}	115	2016
	CS	InAs/GaSb	MWIR LED: 6.7 W cm^{-2} sr^{-1}	193	2017
	SS	MoS_2	PL emission is quenched >50% with respect to that at unstrained interfaces	125	2019
	MS	$MoSe_2$/WS_2	Tunable PL peaks around ~0.1 eV	164	2019
	MS	WSe_2–$MoSe_2$ (0°)	100-fold intensity enhancement of emission, spectrum width of 2 meV, 2000 of Q-factor	170	2019
	MS	Photonic crystal	Bandwidth of ~0.000091 nm, lasing threshold of ~6 kW cm^{-2}	171	2021
	MS	TBG (17.5°)	5-Time enhancement in PL	197	2019
Topological properties	SS	Graphene wrinkle	A modulated short-range (~1–10 nm) pseudo-gauge field (~100 T)	77	2021
	SS	Graphene/h-BN	Pseudo-magnetic fields up to ~800 T	202	2020
	MS	h-BN	Ferroelectric with oppositely polarized dipoles	200	2021

the Gerischer–Marcus electron transfer theory analysis and electronic structure calculations, they believed that the variant distribution of DOS in energy gap leads to different reactivities. In 2018, the chemical reaction research of MSs is further extended to TTG materials.[192] The 30°–30° TTG displayed the highest phenyl radical grafting speed.

4. Opportunities and challenges

The appearance of 2DSs provides a platform for expanding the properties and applications of 2D materials, such as in the field of electronics or optoelectronics. Although this concept is drawn from earlier knowledge of conventional semiconductors, the atomic lattices and unique properties of 2D materials bring new opportunities for their development. In particular, when the introduction of interfacial moiré properties brings spintronics and twistronics into public horizon, 2DSs cannot be regarded as a brief imitation and expansion of traditional materials and structures. Table 1 summarizes the application status of 2DSs in different fields. Most of the work (~70%) took place within the last five years, indicating an emerging attractive field and broad prospects in the further.[193–202]

However, this field is still far from developed and it faces many challenges for development. To simply judge the current status and future trend, we evaluate different 2DSs from six aspects (Fig. 12). Two main issues are primarily believed to be addressed after in-depth analysis. First, high-quality, wafer-scale and convenient preparation of 2DSs is a basic for further development. This is consistent with the current problems faced by the preparation of 2D materials and their heterostructures, while the more complex architectures of 2DSs face more serious requirements. Taking the MS as an example, its properties are directly impacted by the material type, stacking order, twisted angle, interfacial coupling and other factors. Preparing an MS sample design is undoubtedly full of challenges if all the above factors are taken into account. Similarly, when preparing CSs, the preparation efficiency and alternative material types need to be considered; the fabrication accuracy of micro/nanostructures and compatibility with 2D materials should be concerned in SSs preparation. In general, self-assembly technique has great potential due to the rapid and high-quality preparation of materials, and the integration of multiple preparation technologies will be the trend for development.[203–206]

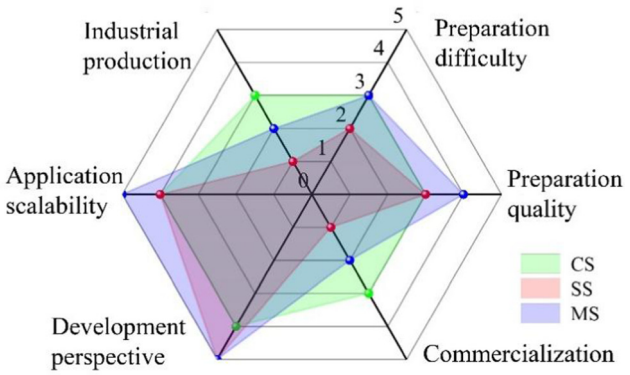

Fig. 12 Comparison diagram of different 2DSs in full scales. For each aspect, we will evaluate it on a scale of 1 to 5.

Second, theoretical prediction, including the construction of physical model and simplified calculation, of 2DSs' properties is another key to promote the development. The initial research on the properties of CSs is indeed based on the expansion of traditional knowledge, but the new forms of 2DSs also bring much unpredictability to novel phenomena. For example, the research on luminescence performance of CSs in recent years is still a recurrence of multiple QW model. It is not completely reasonable to only consider the influence of band offsets but ignore other factors such as the moiré potential, correlated states, chirality and topology in materials. There are no strict structural boundaries for different 2DSs in principle, but it is necessary to open up new paths to comprehensively consider the above factors and obtain predicted results quickly. The theoretical simulation that relies on traditional first-principles calculation will face great computational pressure.[177,207]

In conclusion, this review introduces the common 2DSs from an overall perspective. We reorganize the existing classifications, and mainly focus on the preparation methods, properties and applications. If the 2DSs are applied practically, how to realize their industrial preparation and predict their properties conveniently are two key problems. Although many challenges exist, such new conceptional materials are still attractive because of the more versatile manipulation of material properties. It can be predicted that the related research in theory and experiment will develop in more diversified 2DSs.

Conflicts of interest

The authors declare no conflict of interest.

Acknowledgements

The authors acknowledge financial support from the Foundation of Jilin Educational Committee (JJKH20221151KJ), the National Natural Science Foundation of China (12274065 and 11804334), and the Fundamental Research Funds for the Central Universities (2412021QD004).

Notes and references

1 L. Esaki and R. Tsu, *IBM J. Res. Dev.*, 1970, **14**, 61.
2 L. Esaki and L. Chang, *Phys. Rev. Lett.*, 1974, **33**, 495.
3 F. F. So and S. R. Forrest, *Phys. Rev. Lett.*, 1991, **66**, 2649.
4 G. A. Sai-Halasz, R. Tsu and L. Esaki, *Appl. Phys. Lett.*, 1977, **30**, 651.
5 L. W. Whitlow and T. Hirano, *J. Appl. Phys.*, 1995, **78**, 5460.
6 G. Rijnders and D. H. A. Blank, *Nature*, 2005, **433**, 369–370.
7 T. C. Harman, P. J. Taylor, M. P. Walsh and B. E. LaForge, *Science*, 2002, **297**, 2229–2232.
8 R. Ramesh and D. G. Schlom, *Nat. Rev. Mater.*, 2019, **4**, 257–268.

9 P. Chen, Z. Zhang, X. Duan and X. Duan, *Chem. Soc. Rev.*, 2018, **47**, 3129–3151.
10 Y. Huang, J. Liang, C. Wang, S. Yin, W. Fu, H. Zhu and C. Wan, *Chem. Soc. Rev.*, 2020, **49**, 6866–6883.
11 Y. K. Ryu, R. Frisenda and A. Castellanos-Gomez, *Chem. Commun.*, 2019, **55**, 11498–11510.
12 K. S. Novoselov, A. K. Geim, S. V. Morozov, D. Jiang, Y. Zhang, S. V. Dubonos, I. V. Grigorieva and A. A. Firsov, *Science*, 2004, **306**, 666–669.
13 C. Chang, W. Chen, Y. Chen, Y. Chen, Y. Chen, F. Ding, C. Fan, H. Fan, Z. Fan, C. Gong, Y. Gong, Q. He, X. Hong, S. Hu, W. Hu, W. Huang, Y. Huang, W. Ji, D. Li, L. J. Li, Q. Li, L. Lin, C. Ling, M. Liu, N. Liu, Z. Liu, K. P. Loh, J. Ma, F. Miao, H. Peng, M. Shao, L. Song, S. Su, S. Sun, C. Tan, Z. Tang, D. Wang, H. Wang, J. Wang, X. Wang, X. Wang, A. T. S. Wee, Z. Wei, Y. Wu, Z. S. Wu, J. Xiong, Q. Xiong, W. Xu, P. Yin, H. Zeng, Z. Zeng, T. Zhai, H. Zhang, H. Zhang, Q. Zhang, T. Zhang, X. Zhang, L. D. Zhao, M. Zhao, W. Zhao, Y. Zhao, K. G. Zhou, X. Zhou, Y. Zhou, H. Zhu, H. Zhang and Z. Liu, *Acta Phys. Chim. Sin.*, 2021, **37**, 2108017.
14 K. Khan, A. K. Tareen, M. Aslam, R. Wang, Y. Zhang, A. Mahmood, Z. Ouyang, H. Zhang and Z. Guo, *J. Mater. Chem. C*, 2020, **8**, 387–440.
15 C. Liu, H. Chen, S. Wang, Q. Liu, Y. G. Jiang, D. W. Zhang, M. Liu and P. Zhou, *Nat. Nanotechnol.*, 2020, **15**, 545–557.
16 Y. Liu, N. O. Weiss, X. Duan, H. C. Cheng, Y. Huang and X. Duan, *Nat. Rev. Mater.*, 2016, **1**, 16042.
17 Y. Liu, Y. Huang and X. Duan, *Nature*, 2019, **567**, 323–333.
18 A. K. Geim and I. V. Grigorieva, *Nature*, 2013, **499**, 419–425.
19 C. Wang, Q. He, U. Halim, Y. Liu, E. Zhu, Z. Lin, H. Xiao, X. Duan, Z. Feng, R. Cheng, N. O. Weiss, G. Ye, Y. C. Huang, H. Wu, H. C. Cheng, I. Shakir, L. Liao, X. Chen, W. A. Goddard III, Y. Huang and X. Duan, *Nature*, 2018, **555**, 231–236.
20 S. Xie, L. Tu, Y. Han, L. Huang, K. Kang, K. U. Lao, P. Poddar, C. Park, D. A. Muller, R. A. DiStasio Jr and J. Park, *Science*, 2018, **359**, 1131–1136.
21 Y. Cao, V. Fatemi, S. Fang, K. Watanabe, T. Taniguchi, E. Kaxiras and P. Jarillo-Herrero, *Nature*, 2018, **556**, 43–50.
22 Y. Cao, V. Fatemi, A. Demir, S. Fang, S. L. Tomarken, J. Y. Luo, J. D. Sanchez-Yamagishi, K. Watanabe, T. Taniguchi, E. Kaxiras, R. C. Ashoori and P. Jarillo-Herrero, *Nature*, 2018, **556**, 80–84.
23 J. Wang, M. Wang, F. Xu, B. Liu, J. Lang, N. Zhang, X. Kang, Z. Qin, X. Yang, X. Wang, W. Ge and B. Shen, *Light: Sci. Appl.*, 2022, **11**, 71.
24 G. C. Osbourn, *J. Appl. Phys.*, 1982, **53**(3), 1586.
25 S. Cai, D. Breid, A. J. Crosby, Z. Suo and J. W. Hutchinson, *J. Mech. Phys. Solids*, 2011, **59**, 1094–1114.
26 J. Mao, S. P. Milovanović, M. Anđelković, X. Lai, Y. Cao, K. Watanabe, T. Taniguchi, L. Covaci, F. M. Peeters, A. K. Geim, Y. Jiang and E. Y. Andrei, *Nature*, 2020, **584**, 215.
27 C. Forsythe, X. Zhou, K. Watanabe, T. Taniguchi, A. Pasupathy, P. Moon, M. Koshino, P. Kim and C. R. Dean, *Nat. Nanotechnol.*, 2018, **13**, 566.
28 B. S. Jessen, L. Gammelgaard, M. R. Thomsen, D. M. A. Mackenzie, J. D. Thomsen, J. M. Caridad, E. Duegaard, K. Watanabe, T. Taniguchi, T. J. Booth, T. G. Pedersen, A. P. Jauho and P. Bøggild, *Nat. Nanotechnol.*, 2019, **14**, 340–346.
29 R. Bistritzer and A. H. MacDonald, *Proc. Natl. Acad. Sci. U. S. A.*, 2011, **108**, 12233.
30 E. Y. Andrei and A. H. MacDonald, *Nat. Mater.*, 2020, **19**, 1265–1275.
31 D. Huang, J. Choi, C. K. Shih and X. Li, *Nat. Nanotechnol.*, 2022, **17**, 227–238.
32 X. G. Gao, X. K. Li, W. Xin, X. D. Chen, Z. B. Liu and J. G. Tian, *Nanophotonics*, 2020, **9**, 1717.
33 F. Withers, D. Pozo-Zamudio, A. Mishchenko, A. Rooney, A. Gholinia, K. Watanabe, T. Taniguchi, S. J. Haigh, A. Geim, A. Tartakovskii and K. S. Novoselov, *Nat. Mater.*, 2015, **14**, 301.
34 G. Prando, *Nat. Nanotechnol.*, 2017, **12**, 191.
35 Y. Niu, J. Villalva, R. Frisenda, G. Sanchez-Santolino, L. Ruiz-González, E. M. Pérez, M. García-Hernández, E. Burzurí and A. Castellanos-Gomez, *2D Mater.*, 2019, **6**, 035023.
36 H. W. Guo, Z. Hu, Z. B. Liu and J. G. Tian, *Adv. Funct. Mater.*, 2021, **31**, 2007810.
37 L. Li, R. Ma, Y. Ebina, K. Fukuda, K. Takada and T. Sasaki, *J. Am. Chem. Soc.*, 2007, **129**, 8000–8007.
38 G. Li, A. Luican, J. M. B. Lopes dos Santos, A. H. Castro Neto, A. Reina, J. Kong and E. Y. Andrei, *Nat. Phys.*, 2010, **6**, 109–113.
39 S. J. Haigh, A. Gholinia, R. Jalil, S. Romani, L. Britnell, D. C. Elias, K. S. Novoselov, L. A. Ponomarenko, A. K. Geim and R. Gorbachev, *Nat. Mater.*, 2012, **11**, 764–767.
40 R. Ma, X. Liu, J. Liang, Y. Bando and T. Sasaki, *Adv. Mater.*, 2014, **26**, 4173–4178.
41 B. W. Li, M. Osada, Y. Ebina, S. Ueda and T. Sasaki, *J. Am. Chem. Soc.*, 2016, **138**, 7621–7625.
42 Z. Zhang, P. Chen, X. Duan, K. Zang, J. Luo and X. Duan, *Science*, 2017, **357**, 788–792.
43 Y. Dai, X. Ren, J. Zhang, J. Liu, H. Liu, W. Ho, X. Dai, C. Jin and M. Xie, *ACS Appl. Mater. Interfaces*, 2019, **11**, 43766–43773.
44 P. Xiong, X. Zhang, H. Wan, S. Wang, Y. Zhao, J. Zhang, D. Zhou, W. Gao, R. Ma, T. Sasaki and G. Wang, *Nano Lett.*, 2019, **19**, 4518–4526.
45 Y. Guo, Q. Chen, A. Nie, H. Yang, W. Wang, J. Su, S. Wang, Y. Liu, S. Wang, H. Li, Z. Liu and T. Zhai, *ACS Nano*, 2020, **14**, 1635–1644.
46 M. Liu, K. Hisama, Y. Zheng, M. Maruyama, S. Seo, A. Anisimov, T. Inoue, E. I. Kauppinen, S. Okada, S. Chiashi, R. Xiang and S. Maruyama, *ACS Nano*, 2021, **15**, 8418–8426.
47 B. Zhao, Z. Wan, Y. Liu, J. Xu, X. Yang, D. Shen, Z. Zhang, C. Guo, Q. Qian, J. Li, R. Wu, Z. Lin, X. Yan, B. Li, Z. Zhang, H. Ma, B. Li, X. Chen, Y. Qiao, I. Shakir, Z. Almutairi, F. Wei, Y. Zhang, X. Pan, Y. Huang, Y. Ping, X. Duan and X. Duan, *Nature*, 2021, **591**, 385–390.

48 Z. Lin, Z. Wan, F. Song, B. Huang, C. Jia, Q. Qian, J. S. Kang, Y. Wu, X. Yan, L. Peng, C. Wan, J. Zhou, Z. Sofer, I. Shakir, Z. Almutairi, S. Tolbert, X. Pan, Y. Hu, Y. Huang and X. Duan, *Chem*, 2021, **7**, 1887–1902.
49 Y. Deng, X. Xi, Y. Xia, Y. Cao, S. Xue, S. Wan, A. Dong and D. Yang, *Adv. Mater.*, 2022, **34**, 2109145.
50 X. Wang, Y. Zhao, X. Kong, Q. Zhang, H. K. Ng, S. X. Lim, Y. Zheng, X. Wu, K. Watanabe, Q. H. Xu, T. Taniguchi, G. Eda, K. E. J. Goh, S. Jin, K. P. Loh, F. Ding, W. Sun and C. H. Sow, *ACS Nano*, 2022, **16**, 8172–8180.
51 V. Nicolosi, M. Chhowalla, M. G. Kanatzidis, M. S. Strano and J. N. Coleman, *Science*, 2013, **340**, 1226419.
52 S. B. Desai, S. R. Madhvapathy, M. Amani, D. Kiriya, M. Hettick, M. Tosun, Y. Zhou, M. Dubey, J. W. Ager III, D. Chrzan and A. Javey, *Adv. Mater.*, 2016, **28**, 4053–4058.
53 F. Liu, W. Wu, Y. Bai, S. H. Chae, Q. Li, J. Wang, J. Hone and X. Y. Zhu, *Science*, 2020, **367**, 903–906.
54 Y. Huang, Y. H. Pan, R. Yang, L. H. Bao, L. Meng, H. L. Luo, Y. Q. Cai, G. D. Liu, W. J. Zhao, Z. Zhou, L. M. Wu, Z. L. Zhu, M. Huang, L. W. Liu, L. Liu, P. Cheng, K. H. Wu, S. B. Tian, C. Z. Gu, Y. G. Shi, Y. F. Guo, Z. G. Cheng, J. P. Hu, L. Zhao, G. H. Yang, E. Sutter, P. Sutter, Y. L. Wang, W. Ji, X. J. Zhou and H. J. Gao, *Nat. Commun.*, 2020, **11**, 1.
55 G. Liu, Z. Tian, Z. Yang, Z. Xue, M. Zhang, X. Hu, Y. Wang, Y. Yang, P. K. Chu, Y. Mei, L. Liao, W. Hu and Z. Di, *Nat. Electron.*, 2022, **5**, 275–280.
56 C. R. Dean, A. F. Young, I. Meric, C. Lee, L. Wang, S. Sorgenfrei, K. Watanabe, T. Taniguchi, P. Kim, K. L. Shepard and J. Hone, *Nat. Nanotechnol.*, 2010, **5**, 722–726.
57 Y. Jiang, J. Mao, J. Duan, X. Lai, K. Watanabe, T. Taniguchi and E. Y. Andrei, *Nano Lett.*, 2017, **17**, 2839.
58 H. Kum, D. Lee, W. Kong, H. Kim, Y. Park, Y. Kim, Y. Baek, S. H. Bae, K. Lee and J. Kim, *Nat. Electron.*, 2019, **2**, 439–450.
59 X. Ma, Q. Liu, D. Xu, Y. Zhu, S. Kim, Y. Cui, L. Zhong and M. Liu, *Nano Lett.*, 2017, **17**, 6961–6967.
60 M. Liao, Z. Wei, L. Du, Q. Wang, J. Tang, H. Yu, F. Wu, J. Zhao, X. Xu, B. Han, K. Liu, P. Gao, T. Polcar, Z. Sun, D. Shi, R. Yang and G. Zhang, *Nat. Commun.*, 2020, **11**, 1.
61 W. S. Leong, H. Wang, J. Yeo, F. J. Martin-Martinez, A. Zubair, P. C. Shen, Y. Mao, T. Palacios, M. J. Buehler, J. Y. Hong and J. Kong, *Nat. Commun.*, 2019, **10**, 1.
62 Q. Tao, R. Wu, Q. Li, L. Kong, Y. Chen, J. Jiang, Z. Lu, B. Li, W. Li, Z. Li, L. Liu, X. Duan, L. Liao and Y. Liu, *Nat. Commun.*, 2021, **12**, 1.
63 L. Gao, G. X. Ni, Y. Liu, B. Liu, A. H. Castro Neto and K. P. Loh, *Nature*, 2014, **505**, 190–194.
64 S. J. Yang, J. H. Jung, E. Lee, E. Han, M. Y. Choi, D. Jung, S. Choi, J. H. Park, D. Oh, S. Noh, K. J. Kim, P. Y. Huang, C. C. Hwang and C. J. Kim, *Nano Lett.*, 2022, **22**, 1518–1524.
65 X. Zhou and G. Yu, *ACS Nano*, 2021, **15**, 11040–11065.
66 J. Li, J. Liang, X. Yang, X. Li, B. Zhao, B. Li and X. Duan, *Small*, 2022, 2107059.
67 J. Zhou, J. Lin, X. Huang, Y. Zhou, Y. Chen, J. Xia, H. Wang, Y. Xie, H. Yu, J. Lei, D. Wu, F. Liu, Q. Fu, Q. Zeng, C. H. Hsu, C. Yang, L. Lu, T. Yu, Z. Shen, H. Lin, B. I. Yakobson, Q. Liu, K. Suenaga, G. Liu and Z. Liu, *Nature*, 2018, **556**, 355–359.
68 M. Y. Li, Y. Shi, C. C. Cheng, L. S. Lu, Y. C. Lin, H. L. Tang, M. L. Tsai, C. W. Chu, K. H. Wei, J. H. He, W. H. Chang, K. Suenaga and L. J. Li, *Science*, 2015, **349**, 524–528.
69 K. Liu, L. Zhang, T. Cao, C. Jin, D. Qiu, Q. Zhou, A. Zettl, P. Yang, S. G. Louie and F. Wang, *Nat. Commun.*, 2014, **5**, 1.
70 C. C. Lu, Y. C. Lin, Z. Liu, C. H. Yeh, K. Suenaga and P. W. Chiu, *ACS Nano*, 2013, **7**, 2587–2594.
71 Z. Tan, J. Yin, C. Chen, H. Wang, L. Lin, L. Sun, J. Wu, X. Sun, H. Yang, Y. Chen, H. Peng and Z. Liu, *ACS Nano*, 2016, **10**, 6725–6730.
72 J. Yin, H. Wang, H. Peng, Z. Tan, L. Liao, L. Lin, X. Sun, A. L. Koh, Y. Chen, H. Peng and Z. Liu, *Nat. Commun.*, 2016, **7**, 1.
73 L. Sun, Z. Wang, Y. Wang, L. Zhao, Y. Li, B. Chen, S. Huang, S. Zhang, W. Wang, D. Pei, H. Fang, S. Zhong, H. Liu, J. Zhang, L. Tong, Y. Chen, Z. Li, M. H. Rümmeli, K. S. Novoselov, H. Peng, L. Lin and Z. Liu, *Nat. Commun.*, 2021, **12**, 1.
74 G. Jin, C. S. Lee, O. F. Okello, S. H. Lee, M. Y. Park, S. Cha, S. Y. Seo, G. Moon, S. Y. Min, D. H. Yang, C. Han, H. Ahn, J. Lee, H. Choi, J. Kim, S. Y. Choi and M. H. Jo, *Nat. Nanotechnol.*, 2021, **16**, 1092–1098.
75 R. Xiang, T. Inoue, Y. Zheng, A. Kumamoto, Y. Qian, Y. Sato, M. Liu, D. Tang, D. Gokhale, J. Guo, K. Hisama, S. Yotsumoto, T. Ogamoto, H. Arai, Y. Kobayashi, H. Zhang, B. Hou, A. Anismov, M. Maruyama, Y. Miyata, S. Okada, S. Chiashi, Y. Li, J. Kong, E. I. Kauppinen, Y. Ikuhara, K. Suenaga and S. Maruyama, *Science*, 2020, **367**, 537–542.
76 E. Shi, B. Yuan, S. B. Shiring, Y. Gao, Y. Guo, Akriti, C. Su, M. Lai, P. Yang, J. Kong, B. M. Savoie, Y. Yu and L. Dou, *Nature*, 2020, **580**, 614–620.
77 R. Banerjee, V. H. Nguyen, T. Granzier-Nakajima, L. Pabbi, A. Lherbier, A. R. Binion, J. C. Charlier, M. Terrones and E. W. Hudson, *Nano Lett.*, 2020, **20**, 3113.
78 C. Berger, Z. Song, T. Li, X. Li, A. Y. Ogbazghi, R. Feng, Z. Dai, A. N. Marchenkov, E. H. Conrad, P. N. First and W. A. de. Heer, *J. Phys. Chem. B*, 2004, **108**, 19912–19916.
79 K. V. Emtsev, A. Bostwick, K. Horn, J. Jobst, G. L. Kellogg, L. Ley, J. L. McChesney, T. Ohta, S. A. Reshanov, J. Röhrl, E. Rotenberg, A. K. Schmid, D. Waldmann, H. B. Weber and T. Seyller, *Nat. Mater.*, 2009, **8**, 203–207.
80 A. Davies, J. D. Albar, A. Summerfield, J. C. Thomas, T. S. Cheng, V. V. Korolkov, E. Stapleton, J. Wrigley, N. L. Goodey, C. J. Mellor, A. N. Khlobystov, K. Watanabe, T. Taniguch, C. T. Foxon, L. Eaves, S. V. Novikov and P. H. Beton, *Nano Lett.*, 2018, **18**, 498–504.
81 H. Wen, H. Zhang, Z. Liu, C. Liu, S. Liu, X. Yang, F. Liu and H. Xie, *Nanoscale*, 2018, **10**, 17567.
82 J. Thomas, J. Bradford, T. S. Cheng, A. Summerfield, J. Wrigley, C. J. Mellor, A. N. Khlobystov, C. T. Foxon, L. Eaves, S. V. Novikov and P. H. Beton, *2D Mater.*, 2020, **7**, 035014.

83 J. D. Yao, Z. Q. Zheng and G. W. Yang, *Prog. Mater. Sci.*, 2019, **106**, 100573.
84 Z. Wu, Y. Lyu, Y. Zhang, R. Ding, B. Zheng, Z. Yang, S. P. Lau, X. H. Chen and J. Hao, *Nat. Mater.*, 2021, **20**, 1203–1209.
85 M. Osada, T. Sasaki, K. Ono, Y. Kotani, S. Ueda and K. Kobayashi, *ACS Nano*, 2011, **5**, 6871–6879.
86 K. Kang, K. H. Lee, Y. Han, H. Gao, S. Xie, D. A. Muller and J. Park, *Nature*, 2017, **550**, 229–233.
87 M. Osada, K. Akatsuka, Y. Ebina, H. Funakubo, K. Ono, K. Takada and T. Sasaki, *ACS Nano*, 2010, **4**, 5225–5232.
88 K. Akatsuka, M. A. Haga, Y. Ebina, M. Osada, K. Fukuda and T. Sasaki, *ACS Nano*, 2009, **3**, 1097–1106.
89 B. W. Li, M. Osada, Y. Ebina, K. Akatsuka, K. Fukuda and T. Sasaki, *ACS Nano*, 2014, **8**, 5449–5461.
90 J. C. Ondry, S. Robbennolt, H. Kang, Y. Yan and S. H. Tolbert, *Chem. Mater.*, 2016, **28**, 6105–6117.
91 S. Zhang, P. Huang, J. Wang, Z. Zhuang, Z. Zhang and W. Q. Han, *J. Phys. Chem. Lett.*, 2020, **11**, 1247–1254.
92 L. Wang, K. Takada, A. Kajiyama, M. Onoda, Y. Michiue, L. Zhang, M. Watanabe and T. Sasaki, *Chem. Mater.*, 2003, **15**, 4508.
93 X. Cai, T. C. Ozawa, A. Funatsu, R. Ma, Y. Ebina and T. Sasaki, *J. Am. Chem. Soc.*, 2015, **137**, 2844–2847.
94 P. Xiong, B. Sun, N. Sakai, R. Ma, T. Sasaki, S. Wang, J. Zhang and G. Wang, *Adv. Mater.*, 2020, **32**, 1902654.
95 X. Ge, C. Gu, Z. Yin, X. Wang, J. Tu and J. Li, *Nano Energy*, 2016, **20**, 185–193.
96 P. Xiong, R. Ma, N. Sakai, L. Nurdiwijayanto and T. Sasaki, *ACS Energy Lett.*, 2018, **3**, 997–1005.
97 L. Jiang, J. Duan, J. Zhu, S. Chen and M. Antonietti, *ACS Nano*, 2020, **14**, 2436–2444.
98 L. Wang, D. Wang, X. Y. Dong, Z. J. Zhang, X. F. Pei, X. J. Chen, B. Chen and J. Jin, *Chem. Commun.*, 2011, **47**, 3556–3558.
99 X. Dong, L. Wang, D. Wang, C. Li and J. Jin, *Langmuir*, 2012, **28**, 293–298.
100 J. Xie, X. Sun, N. Zhang, K. Xu, M. Zhou and Y. Xie, *Nano Energy*, 2013, **2**, 65–74.
101 R. Zhao, M. Wang, D. Zhao, H. Li, C. Wang and L. Yin, *ACS Energy Lett.*, 2017, **3**, 132–140.
102 P. Xiong, F. Zhang, X. Zhang, S. Wang, H. Liu, B. Sun, J. Zhang, Y. Sun, R. Ma, Y. Bando, C. Zhou, Z. Liu, T. Sasaki and G. Wang, *Nat. Commun.*, 2020, **11**, 1.
103 P. Xiong, R. Ma, G. Wang and T. Sasaki, *Energy Storage Mater.*, 2019, **19**, 281–298.
104 Y. Li, Y. Liang, F. C. Robles Hernandez, H. Deog Yoo, Q. An and Y. Yao, *Nano Energy*, 2015, **15**, 453.
105 P. Xiong, R. Ma, N. Sakai and T. Sasaki, *ACS Nano*, 2018, **12**, 1768.
106 H. Tian, H. Shao, Y. Chen, X. Fang, P. Xiong, B. Sun, P. H. L. Notten and G. Wang, *Nano Energy*, 2019, **57**, 692–702.
107 P. Jiang, J. Jing, Y. Wang, H. Li, X. He, Y. Chen and W. Liu, *J. Alloys Compd.*, 2020, **812**, 152114.
108 P. Xiong, X. Zhang, F. Zhang, D. Yi, J. Zhang, B. Sun, H. Tian, D. Shanmukaraj, T. Rojo, M. Armand, R. Ma, T. Sasaki and G. Wang, *ACS Nano*, 2018, **12**, 12337.
109 R. Yang, Y. Zhou, Y. Xing, D. Li, D. Jiang, M. Chen, W. Shi and S. Yuan, *Appl. Catal., B*, 2019, **253**, 131–139.
110 N. H. Kwon, S. J. Shin, X. Jin, Y. Jung, G. S. Hwang, H. Kim and S. J. Hwang, *Appl. Catal., B*, 2020, **277**, 119191.
111 Z. Zhang, P. Liu, Y. Song, Y. Hou, B. Xu, T. Liao, H. Zhang, J. Guo and Z. Sun, *Adv. Sci.*, 2022, 2204297.
112 J. Gu, B. Chakraborty, M. Khatoniar and V. M. Menon, *Nat. Nanotechnol.*, 2019, **14**, 1024–1028.
113 M. J. Lee, D. H. Seo, S. M. Kwon, D. Kim, Y. Kim, W. S. Yun, J. H. Cha, H. K. Song, S. Lee and M. Jung, *ACS Nano*, 2020, **14**, 16114–16121.
114 P. Kumar, J. Lynch, B. Song, H. Ling, F. Barrera, K. Kisslinger, H. Zhang, S. B. Anantharaman, J. Digani, H. Zhu, T. H. Choudhury, C. Mcaleese, X. Wang, B. R. Conran, O. Whear, M. J. Motala, M. Snure, C. Muratore, J. M. Redwing, N. R. Glavin, E. A. Stach, A. R. Davoyan and D. Jariwala, *Nat. Nanotechnol.*, 2022, **17**, 182–189.
115 N. Wang, L. Cheng, R. Ge, S. Zhang, Y. Miao, W. Zou, C. Yi, Y. Sun, Y. Cao, R. Yang, Y. Wei, Q. Guo, Y. Ke, M. Yu, Y. Jin, Y. Liu, Q. Ding, D. Di, L. Yang, G. Xing, H. Tian, C. Jin, F. Gao, R. H. Friend and W. Huang, *Nat. Photonics*, 2016, **10**, 699–704.
116 S. Fan, R. Cao, L. Wang, S. Gao, Y. Zhang, X. Yu and H. Zhang, *Sci. China Mater.*, 2021, **64**, 2359–2387.
117 T. P. Broekaert, W. Lee and C. G. Fonstad, *Appl. Phys. Lett.*, 1988, **53**, 1545.
118 F. Capasso and R. A. Kiehl, *J. Appl. Phys.*, 1985, **58**, 1366.
119 P. M. Campbell, A. Tarasov, C. A. Joiner, W. J. Ready and E. M. Vogel, *ACS Nano*, 2015, **9**, 5000–5008.
120 A. Tsen, B. Hunt, Y. Kim, Z. Yuan, S. Jia, R. Cava, J. Hone, P. Kim, C. Dean and A. Pasupathy, *Nat. Phys.*, 2016, **12**, 208–212.
121 A. Devarakonda, H. Inoue, S. Fang, C. Ozsoy-Keskinbora, T. Suzuki, M. Kriener, L. Fu, E. Kaxiras, D. C. Bell and J. G. Checkelsky, *Science*, 2020, **370**, 231–236.
122 Z. Li, Y. Zhao, K. Mu, H. Shan, Y. Guo, J. Wu, Y. Su, Q. Wu, Z. Sun, A. Zhao, X. Cui, C. Wu and Y. Xie, *J. Am. Chem. Soc.*, 2017, **139**, 16398–16404.
123 Z. Li, X. Zhang, X. Zhao, J. Li, T. S. Herng, H. Xu, F. Lin, P. Lyu, X. Peng, W. Yu, X. Hai, C. Chen, H. Yang, J. Martin and J. Lu, *Adv. Mater.*, 2020, **32**, 1907645.
124 G. Wang, Z. Dai, J. Xiao, S. Feng, C. Weng, L. Liu, Z. Xu, R. Huang and Z. Zhang, *Phys. Rev. Lett.*, 2019, **123**, 116101.
125 B. Liu, Q. Liao, X. Zhang, J. Du, Y. Ou, J. Xiao, Z. Kang, Z. Zhang and Y. Zhang, *ACS Nano*, 2019, **13**, 9057–9066.
126 H. Kim, S. Z. Uddin, D. H. Lien, M. Yeh, N. S. Azar, S. Balendhran, T. Kim, N. Gupta, Y. Rho, C. P. Grigoropoulos, K. B. Crozier and A. Javey, *Nature*, 2021, **596**, 232–237.
127 J. Quereda, P. San-Jose, V. Parente, L. Vaquero-Garzon, A. J. Molina-Mendoza, N. Agraït, G. Rubio-Bollinger, F. Guinea, R. Roldán and A. Castellanos-Gomez, *Nano Lett.*, 2016, **16**, 2931–3937.
128 V. Torres, P. Silva, E. De Souza, L. Silva and D. Bahamon, *Phys. Rev. B*, 2019, **100**, 205411.

129 R. X. Sun, Q. Q. Guo, H. W. Guo, X. Q. Yan, Z. B. Liu and J. G. Tian, *J. Phys. Chem. Lett.*, 2020, **11**, 5059–5067.
130 K. J. Lee, W. Xin and C. Guo, *Phys. Rev. B*, 2020, **101**, 195407.
131 K. J. Lee, W. Xin, C. Fann, X. Ma, F. Xing, J. Liu, J. Zhang, M. Elkabbash and C. Guo, *Phys. Rev. B*, 2020, **101**, 041405.
132 C. H. Chen, W. W. Li, Y. M. Chang, C. Y. Lin, S. H. Yang, Y. Xu and Y. F. Lin, *Phys. Rev. Appl.*, 2018, **10**, 044047.
133 Z. Wang, F. Liu and M. Chou, *Nano Lett.*, 2012, **12**, 3833–3838.
134 C. R. Dean, L. Wang, P. Maher, C. Forsythe, F. Ghahari, Y. Gao, J. Katoch, M. Ishigami, P. Moon, M. Koshino, T. Taniguchi, K. Watanabe and K. L. Shepard, *Nature*, 2013, **497**, 598–602.
135 Y. Li, S. Dietrich, C. Forsythe, T. Taniguchi, K. Watanabe, P. Moon and C. R. Dean, *Nat. Nanotechnol.*, 2021, **16**, 525–530.
136 H. Lin, B. C. Sturmberg, K. T. Lin, Y. Yang, X. Zheng, T. K. Chong, C. M. de Sterke and B. Jia, *Nat. Photonics*, 2019, **13**, 270–276.
137 H. Yan, X. Li, B. Chandra, G. Tulevski, Y. Wu, M. Freitag, W. Zhu, P. Avouris and F. Xia, *Nat. Nanotechnol.*, 2012, **7**, 330–334.
138 J. L. Dos Santos, N. Peres and A. C. Neto, *Phys. Rev. Lett.*, 2007, **99**, 256802.
139 H. Tang, F. Du, S. Carr, C. DeVault, O. Mello and E. Mazur, *Light: Sci. Appl.*, 2021, **10**, 1–8.
140 Y. Xiao, J. Liu and L. Fu, *Matter*, 2020, **3**, 1142–1161.
141 S. Carr, D. Massatt, S. Fang, P. Cazeaux, M. Luskin and E. Kaxiras, *Phys. Rev. B*, 2017, **95**, 075420.
142 S. Carr, S. Fang and E. Kaxiras, *Nat. Rev. Mater.*, 2020, **5**, 748–763.
143 J. Yang, G. Chen, T. Han, Q. Zhang, Y. H. Zhang, L. Jiang, B. Lyu, H. Li, K. Watanabe, T. Taniguchi, Z. Shi, T. Senthil, Y. Zhang, F. Wang and L. Ju, *Science*, 2022, **375**, 1295–1299.
144 E. Codecido, Q. Wang, R. Koester, S. Che, H. Tian, R. Lv, S. Tran, K. Watanabe, T. Taniguchi, F. Zhang, M. Bockrath and C. N. Lau, *Sci. Adv.*, 2019, **5**, eaaw9770.
145 Y. Cao, D. Rodan-Legrain, O. Rubies-Bigorda, J. M. Park, K. Watanabe, T. Taniguchi and P. Jarillo-Herrero, *Nature*, 2020, **583**, 215–220.
146 J. M. Park, Y. Cao, K. Watanabe, T. Taniguchi and P. Jarillo-Herrero, *Nature*, 2021, **590**, 249–255.
147 Y. Cao, J. M. Park, K. Watanabe, T. Taniguchi and P. Jarillo-Herrero, *Nature*, 2021, **595**, 526–531.
148 Z. Hao, A. M. Zimmerman, P. Ledwith, E. Khalaf, D. H. Najafabadi, K. Watanabe, T. Taniguchi, A. Vishwanath and P. Kim, *Science*, 2021, **371**, 1133–1138.
149 W. Xin, X. K. Li, X. L. He, B. W. Su, X. Q. Jiang, K. X. Huang, X. F. Zhou, Z. B. Liu and J. G. Tian, *Adv. Mater.*, 2018, **30**, 1704653.
150 W. Xin, H. B. Jiang, X. K. Li, X. F. Zhou, J. L. Lu, J. J. Yang, C. Guo, Z. B. Liu and J. G. Tian, *Adv. Mater. Interfaces*, 2018, **5**, 1800964.
151 P. K. Srivastava, Y. Hassan, D. J. de Sousa, Y. Gebredingle, M. Joe, F. Ali, Y. Zheng, W. J. Yoo, S. Ghosh, J. T. Teherani, B. Singh, T. Low and C. Lee, *Nat. Electron.*, 2021, **4**, 269.
152 P. Moon and M. Koshino, *Phys. Rev. B: Condens. Matter Mater. Phys.*, 2013, **87**, 205404.
153 X. D. Chen, W. Xin, W. S. Jiang, Z. B. Liu, Y. Chen and J. G. Tian, *Adv. Mater.*, 2016, **28**, 2563–2570.
154 K. Kim, S. Coh, L. Z. Tan, W. Regan, J. M. Yuk, E. Chatterjee, M. Crommie, M. L. Cohen, S. G. Louie and A. Zettl, *Phys. Rev. Lett.*, 2012, **108**, 246103.
155 J. Campos-Delgado, L. G. Cançado, C. A. Achete, A. Jorio and J. P. Raskin, *Nano Res.*, 2013, **6**, 269–274.
156 S. Ha, N. H. Park, H. Kim, J. Shin, J. Choi, S. Park, J. Y. Moon, K. Chae, J. Jung, J. H. Lee, Y. Yoo, J. Y. Park, K. J. Ahn and D. Y. Eom, *Light: Sci. Appl.*, 2021, **2**, 19.
157 C. J. Kim, A. Sánchez-Castillo, Z. Ziegler, Y. Ogawa, C. Noguez and J. Park, *Nat. Nanotechnol.*, 2016, **11**, 520.
158 Z. Zheng, Y. Song, Y. W. Shan, W. Xin and J. L. Cheng, *Phys. Rev. B*, 2022, **105**, 085407.
159 X. Wang, C. Xiao, H. Park, J. Zhu, C. Wang, T. Taniguchi, K. Watanabe, J. Yan, D. Xiao, D. R. Gamelin, W. Yao and X. Xu, *Nature*, 2022, **604**, 468–473.
160 G. Hu, Q. Ou, G. Si, Y. Wu, J. Wu, Z. Dai, A. Krasnok, Y. Mazor, Q. Zhang, Q. Bao, C. W. Qiu and A. AlÙ, *Nature*, 2020, **582**, 209–213.
161 M. Chen, X. Lin, T. H. Dinh, Z. Zheng, J. Shen, Q. Ma, H. Chen, P. Jarillo-Herrero and S. Dai, *Nat. Mater.*, 2020, **19**, 1307–1311.
162 A. M. Van Der Zande, J. Kunstmann, A. Chernikov, D. A. Chenet, Y. You, X. Zhang, P. Y. Huang, T. C. Berkelbach, L. Wang, F. Zhang, M. S. Hybertsen, D. A. Muller, D. R. Reichman, T. F. Heinz and J. C. Hone, *Nano Lett.*, 2014, **14**, 3869–3875.
163 J. Kunstmann, F. Mooshammer, P. Nagler, A. Chaves, F. Stein, N. Paradiso, G. Plechinger, C. Strunk, C. Schüller, G. Seifert, D. R. Reichman and T. Korn, *Nat. Phys.*, 2018, **14**, 801–805.
164 E. M. Alexeev, D. A. Ruiz-Tijerina, M. Danovich, M. J. Hamer, D. J. Terry, P. K. Nayak, S. Ahn, S. Pak, J. Lee, J. I. Sohn, M. R. Molas, M. Koperski, K. Watanabe, T. Taniguchi, K. S. Novoselov, R. V. Gorbachev, H. S. Shin, V. L. Falko and A. L. Tartakovskii, *Nature*, 2019, **567**, 81–86.
165 H. Zhu, J. Wang, Z. Gong, Y. D. Kim, J. Hone and X. Y. Zhu, *Nano Lett.*, 2017, **17**, 3591–3598.
166 J. Choi, M. Florian, A. Steinhoff, D. Erben, K. Tran, D. S. Kim, L. Sun, J. Quan, R. Claassen, S. Majumder, J. A. Hollingsworth, T. Taniguchi and K. Watanable, *Phys. Rev. Lett.*, 2021, **126**, 047401.
167 C. Jin, E. C. Regan, A. Yan, M. Iqbal Bakti Utama, D. Wang, S. Zhao, Y. Qin, S. Yang, Z. Zheng, S. Shi, K. Watanabe, T. Taniguchi, S. Tongay, A. Zettl and F. Wang, *Nature*, 2019, **567**, 76–80.
168 K. L. Seyler, P. Rivera, H. Yu, N. P. Wilson, E. L. Ray, D. G. Mandrus, J. Yan, W. Yao and X. Xu, *Nature*, 2019, **567**, 66–70.
169 K. Tran, G. Moody, F. Wu, X. Lu, J. Choi, K. Kim, A. Rai, D. A. Sanchez, J. Quan, A. Singh, J. Embley, A. Zepeda, M. Campbell, T. Autry, T. Taniguchi, K. Watanabe, N. Lu, S. K. Banerjee, K. L. Silverman, S. Kim, E. Tutuc, L. Yang, A. H. Macdonald and X. Li, *Nature*, 2019, **567**, 71–75.

170 E. Y. Paik, L. Zhang, G. W. Burg, R. Gogna, E. Tutuc and H. Deng, *Nature*, 2019, **576**, 80–84.
171 X. R. Mao, Z. K. Shao, H. Y. Luan, S. L. Wang and R. M. Ma, *Nat. Nanotechnol.*, 2021, **16**, 1099–1105.
172 M. Wu, X. Qian and J. Li, *Nano Lett.*, 2014, **14**, 5350–5357.
173 Y. Wang, Y. Lan, Q. Song, F. Vogelbacher, T. Xu, Y. Zhan, M. Li, W. E. Sha and Y. Song, *Adv. Mater.*, 2021, **33**, 2008091.
174 W. Xin, X. D. Chen, Z. B. Liu, W. S. Jiang, X. G. Gao, X. Q. Jiang, Y. Chen and J. G. Tian, *Adv. Opt. Mater.*, 2016, **4**, 1703–1710.
175 S. Wu, L. Wang, Y. Lai, W. Y. Shan, G. Aivazian, X. Zhang, T. Taniguchi, K. Watanabe, D. Xiao, C. Dean, J. Hone, Z. Li and X. Xu, *Sci. Adv.*, 2016, **2**, 1600002.
176 B. Deng, C. Ma, Q. Wang, S. Yuan, K. Watanabe, T. Taniguchi, F. Zhang and F. Xia, *Nat. Photonics*, 2020, **14**, 549–553.
177 C. Ma, S. Yuan, P. Cheung, K. Watanabe, T. Taniguchi, F. Zhang and F. Xia, *Nature*, 2022, **604**, 266–272.
178 P. Seifert, X. Lu, P. Stepanov, J. R. N. Durán Retamal, J. N. Moore, K. C. Fong, A. Principi and D. K. Efetov, *Nano Lett.*, 2020, **20**, 3459–3464.
179 T. Akamatsu, T. Ideue, L. Zhou, Y. Dong, S. Kitamura, M. Yoshii, D. Yang, M. Onga, Y. Nakagawa, K. Watanabe, T. Taniguchl, J. Laurienzo, J. Huang, Z. Ye, T. Morlmoto, H. Yuan and Y. Lwasa, *Science*, 2021, **372**, 68–72.
180 Y. Xiong, Y. Wang, R. Zhu, H. Xu, C. Wu, J. Chen, Y. Ma, Y. Liu, Y. Chen, K. Watanabe, T. Tanlguchl, M. Shl, X. Chen, Y. Lu, P. Zhan, Y. Hao and F. Xu, *Sci. Adv.*, 2022, **8**, eabo0375.
181 A. Luican, G. Li, A. Reina, J. Kong, R. Nair, K. S. Novoselov, A. K. Geim and E. Andrei, *Phys. Rev. Lett.*, 2011, **106**, 126802.
182 L. J. Yin, J. B. Qiao, W. X. Wang, W. J. Zuo, W. Yan, R. Xu, R. F. Dou, J. C. Nie and L. He, *Phys. Rev. B: Condens. Matter Mater. Phys.*, 2015, **92**, 201408.
183 K. Uchida, S. Furuya, J. I. Iwata and A. Oshiyama, *Phys. Rev. B: Condens. Matter Mater. Phys.*, 2014, **90**, 155451.
184 D. S. Lee, C. Riedl, T. Beringer, A. C. Neto, K. von Klitzing, U. Starke and J. H. Smet, *Phys. Rev. Lett.*, 2011, **107**, 216602.
185 Y. Liu, J. Rodrigues, Y. Z. Luo, L. Li, A. Carvalho, M. Yang, E. Laksono, J. Lu, Y. Bao, H. Xu, S. J. R. Tan, Z. Qiu, C. H. Sow, Y. P. Feng, A. H. C. Neto, S. Adam, J. Lu and K. P. Loh, *Nat. Nanotechnol.*, 2018, **13**, 828–834.
186 A. Vanossi, C. Bechinger and M. Urbakh, *Nat. Commun.*, 2020, **11**, 4657.
187 Y. Song, D. Mandelli, O. Hod, M. Urbakh, M. Ma and Q. Zheng, *Nat. Mater.*, 2018, **17**, 894–899.
188 S. Zhang, Q. Yao, L. Chen, C. Jiang, T. Ma, H. Wang, X. Q. Feng and Q. Li, *Phys. Rev. Lett.*, 2022, **128**, 226101.
189 W. Ren, Y. Ouyang, P. Jiang, C. Yu, J. He and J. Chen, *Nano Lett.*, 2021, **21**, 2634–2641.
190 L. Liao, H. Wang, H. Peng, J. Yin, A. L. Koh, Y. Chen, Q. Xie, H. Peng and Z. Liu, *Nano Lett.*, 2015, **15**, 5585–5589.
191 Y. Ding, Q. Peng, L. Gan, R. Wu, X. Ou, Q. Zhang and Z. Luo, *Chem. Mater.*, 2016, **28**, 1034–1039.
192 Y. Ding, R. Wu, I. H. Abidi, H. Wong, Z. Liu, M. Zhuang, L. Y. Gan and Z. Luo, *ACS Appl. Mater. Interfaces*, 2018, **10**, 23424–23431.
193 A. Muhowski, R. Ricker, T. Boggess and J. Prineas, *Appl. Phys. Lett.*, 2017, **111**, 243509.
194 L. Xie, L. Wang, W. Zhao, S. Liu, W. Huang and Q. Zhao, *Nat. Commun.*, 2021, **12**, 5070.
195 Z. Jiang, W. Zhou, A. Hong, M. Guo, X. Luo and C. Yuan, *ACS Energy Lett.*, 2019, **4**, 2830–2835.
196 M. Yankowitz, S. Chen, H. Polshyn, Y. Zhang, K. Watanabe, T. Taniguchi, D. Graf, A. F. Young and C. R. Dean, *Science*, 2019, **363**, 1059–1064.
197 H. Patel, L. Huang, C. J. Kim, J. Park and M. W. Graham, *Nat. Commun.*, 2019, **10**, 1445.
198 J. Wang, M. Han, Q. Wang, Y. Ji, X. Zhang, R. Shi, Z. Wu, L. Zhang, A. Amini, L. Guo, N. Wang, J. Lin and C. Cheng, *ACS Nano*, 2021, **15**, 6633–6644.
199 W. Choi, S. Hong, Y. Jeong, Y. Cho, H. G. Shin, J. H. Park, Y. Yi and S. Im, *Adv. Funct. Mater.*, 2021, **31**, 2009436.
200 C. Woods, P. Ares, H. Nevison-Andrews, M. Holwill, R. Fabregas, F. Guinea, A. Geim, K. Novoselov, N. Walet and L. Fumagalli, *Nat. Commun.*, 2021, **12**, 347.
201 H. Li, A. W. Contryman, X. Qian, S. M. Ardakani, Y. Gong, X. Wang, J. M. Weisse, C. H. Lee, J. Zhao, P. M. Ajayan, J. Li, H. C. Manoharan and X. Zheng, *Nat. Commun.*, 2015, **6**, 7381.
202 C. C. Hsu, M. Teague, J. Q. Wang and N. C. Yeh, *Sci. Adv.*, 2020, **6**, aat9488.
203 R. Bian, C. Li, Q. Liu, G. Cao, Q. Fu, P. Meng, J. Zhou, F. Liu and Z. Liu, *Natl. Sci. Rev.*, 2022, **9**, nwab164.
204 P. J. Santos, P. A. Gabrys, L. Z. Zornberg, M. S. Lee and R. J. Macfarlane, *Nature*, 2021, **591**, 586–591.
205 Y. Gong, H. Yuan, C. L. Wu, P. Tang, S. Z. Yang, A. Yang, G. Li, B. Liu, J. van de Groep, M. L. Brongersma, M. F. Chisholm, S. Zhang, W. Zhou and Y. Cui, *Nat. Nanotechnol.*, 2018, **13**, 294–299.
206 H. Yin, K. Xing, Y. Zhang, D. A. S. Dissanayake, Z. Lu, H. Zhao, Z. Zeng, J. H. Yun, D. C. Qi and Z. Yin, *Chem. Soc. Rev.*, 2021, **50**, 6423–6482.
207 H. Ren, Z. Wan and X. Duan, *Natl. Sci. Rev.*, 2022, **9**, nwab166.

